This article has been accepted for publication in Current Biology (Published by Elsevier) and should be cited as:

Stefanie S.Schmieder, Claire E. Stanley, Andrzej Rzepiela, Dirk van Swaay, Jerica Sabotič, Simon F. Nørrelykke, Andrew J. deMello, Markus Aebi, Markus Künzler. 2019. Bidirectional propagation of signals and nutrients in fungal networks via specialized hyphae. *Current Biology*, 29: 217-228.

First Published: 3 January 2019 https://doi.org/10.1016/j.cub.2018.11.058

Bidirectional propagation of signals and nutrients in fungal networks via specialized hyphae

Stefanie S. Schmieder[1,6¶], Claire E. Stanley[2,3¶], Andrzej Rzepiela[4], Dirk van Swaay[2], Jerica Sabotič[5], Simon F. Nørrelykke[4], Andrew J. deMello[2], Markus Aebi[1], Markus Künzler[1*]

[1]Department of Biology, Institute of Microbiology, ETH Zürich, Zürich, Switzerland

[2]Department of Chemistry and Applied Biosciences, Institute for Chemical and Bioengineering, ETH Zürich, Zürich, Switzerland

[3]Present address: Agroecology and Environment Research Division, Agroscope, Zürich, Switzerland

[4]Scientific Center for Optical and Electron Microscopy, ETH Zürich, Switzerland

[5]Department of Biotechnology, Jožef Stefan Institute, Ljubljana, Slovenia

[6]Present address: Division of Gastroenterology, Boston Children's Hospital, Harvard Medical School, Boston, USA

[¶]Contributed equally

*Corresponding author and lead contact:
Markus Künzler
Vladimir-Prelog-Weg 4, HCI F409
CH-8093 Zürich
Switzerland
Tel: +41 44 632 49 25
e-mail: mkuenzle@ethz.ch
ORCID: 0000-0003-1275-0629

Summary

Intercellular distribution of nutrients and coordination of responses to internal and external cues via endogenous signaling molecules are hallmarks of multicellular organisms. Vegetative mycelia of multicellular fungi are syncytial networks of interconnected hyphae resulting from hyphal tip growth, branching and fusion. Such mycelia can reach considerable dimensions and, thus, different parts can be exposed to quite different environmental conditions. Our knowledge about the mechanisms by which fungal mycelia can adjust nutrient gradients or coordinate their defense response to fungivores is scarce, in part due to limitations in technologies currently available for examining different parts of a mycelium over longer time periods at microscopic level. Here, we combined a tailor-made microfluidic platform with time-lapse fluorescence microscopy to visualize the dynamic response of the vegetative mycelium of a basidiomycete to two different stimuli. The microfluidic platform allows simultaneous monitoring at both the colony and single hyphal level. We followed the dynamics of the distribution of a locally administered nutrient analog and the defense response to spatially confined predation by a fungivorous nematode. While both responses of the mycelium were constrained locally, we observed long distance propagation for both the nutrient analog and defense response in a subset of hyphae. This propagation along hyphae occurred in both acropetal and basipetal direction and, intriguingly, the direction was found to alternate every three hours in an individual hypha. These results suggest that multicellular fungi have, as of yet, undescribed mechanisms to coordinate the distribution of nutrients and their behavioral response upon attack by fungivores.

Keywords

Microfluidic platform, mycelial networks, inducible defense response, nutrient distribution

Introduction

Natural environments are heterogeneous in many aspects. Nutrient composition in the soil is subject to spatio-temporal variations, which creates very distinct and ephemeral microhabitats [1]. Fungi cope with this discontinuous nutrient distribution by the formation of a continuous (syncytial) network of arrays of linearly arranged cells (hyphae), referred to as a mycelium, which allows them to access nutrient-rich microhabitats and to achieve nutritional homeostasis within all cells of the multicellular organism [2, 3].

Fungal mycelia grow by tip extension of individual hyphae, resulting in indeterminate radial growth, while secondary and further branches populate intermediary regions to optimize nutrient acquisition [4]. The formation of a network is accomplished by hyphal fusion (anastomosis) [5-7]. Depending on the fungal species, such networks can become quite large, ranging from cubic centimeters to many cubic meters, as is the case for ectomycorrhizal systems or cord-forming basidiomycetes [8]. The network as such can be continuously remodeled and is therefore highly dynamic, adapting to different underlying nutrient conditions, damage or assault by meso-fauna [8-10]. Such network dynamics requires the reallocation of nutrients from different parts of the mycelium to allow, for example, bridging of nutrient-poor areas or damage repair [9-15]. Nutrient reallocation (in the form of radiotracers) through mycelial networks was predominantly examined and observed within cords or rhizomorphs of different basidiomycete species where it is claimed to be important for the sufficient delivery and distribution of metabolically relevant nutrients to growing tips [16-19]. The driving force for this nutrient reallocation was hypothesized to be mainly pressure driven mass flow [20-22]. However, the reported bidirectionality (acropetal and basipetal direction) of nutrient reallocation is difficult to explain with this model [20, 22-24]. Furthermore, the spatial scale at which mycelia operate in nature as a physically or physiologically integrated entity is not known [14].

Besides local fluctuations in physicochemical elements, biotic factors including microbial and faunal communities co-inhabiting a particular microhabitat give rise to considerable environmental variations in space and time. For example, the sessile and heterotrophic lifestyle of fungi entails constraints when encountering competitors, predators or parasites. In order to defend themselves against these

antagonists, fungi have developed an impressive arsenal of toxic metabolites and proteins [25-29]. This defense response in fungi can be induced, as shown by the activation of secondary metabolite gene clusters [30-32]. The model mushroom *Coprinopsis cinerea* induces nematotoxic lectins upon challenge with the fungivorous nematode *Aphelenchus avenae* [33, 34]. Thus far, studies of inducible defense responses of fungal mycelia have focused on transcriptional/translational changes of the entire organism (mycelium). The defense response of individual hyphae, the eventual propagation of these local responses to other parts of the mycelium, as well as the ecological significance of such coordinated behavior, remain to be elucidated [35-37].

In order to understand how the vegetative mycelium of *C. cinerea* responds to local changes in the environment, we developed a microfluidic platform designed to constrain the area of interaction between fungal mycelia and nematodes and visualize events occurring within individual hyphae (Fungal-Nematode-Interaction device, FNI). Microfluidic manipulation of fluid volumes on the microscale has been employed in a multitude of different biological disciplines, notably for the study of whole (living) organisms in recent years [38]. Importantly, our novel FNI platform enables the precise manipulation of the microenvironment, including the addition of nematodes and abiotic stimuli [39], and allows the fungus of interest, growing both within and outside of the confrontation area, to be monitored. In combination with high-resolution, automated imaging techniques, this platform facilitates the study of dynamic biological processes at the cellular level without losing spatial or temporal resolution. We constructed *C. cinerea* reporter strains to visualize and quantify the induction of genes coding for defense proteins upon challenge with nematodes. As a result of combining the reporter strain with the microfluidic platform, we were able to follow the defense response of the fungus in real-time and with single hyphal resolution. The same setup was used to introduce the fluorescent glucose analog 2-NBDG to precise locations within the microfluidic device to follow nutrient transport through the mycelium.

This experimental setup revealed that the transcriptional induction of *C. cinerea* defense genes in response to predation by *A. avenae* is mainly localized to those parts of the vegetative mycelium that are in direct contact with the predator. We could, however, identify a distinct hyphal subtype in the mycelium of this basidiomycete that was capable of propagating the defense response over several millimeters both in

the acropetal and basipetal direction. Remarkably, our time-lapse studies revealed an oscillation of the fluorescence signal with a constant periodicity of approximately 4-6 h within these hyphae. The same hyphal subtype also transported the glucose analog 2-NBDG with similar kinetics, but propagation of the defense signal and transport of 2-NBDG was mutually exclusive when triggered/applied at opposite locations within the device. These findings can be explained by a periodical switch in the direction of solute transport and coordinated opening and closure of septa in these hyphae.

Results

Local and specific defense response of *C. cinerea* against the fungivorous nematode *A. avenae*

To monitor the spatial distribution of the *C. cinerea* defense response upon predation by *A. avenae* with cellular resolution, we first designed a microfluidic device (FNI) in which the access of nematodes to the growing mycelium is restricted to specific regions, namely the "confrontation area" (Figures 1A-B, Figures S1A-B). Spatial restriction is achieved by incorporating constriction channels between the confrontation area and the basipetal and acropetal monitoring areas. Due to their small width and height (10 µm) and long length (500 µm), nematodes cannot enter these channels. We also introduced a control area for examination of non-confronted hyphae of the same mycelial colony. Secondly, we constructed various *C. cinerea* AmBm reporter strains carrying either dTomato or eGFP expression cassettes driven by the promoters of the *cgl2* and *cctx2* genes to visualize the expression of these genes. The expression of both genes is induced in the vegetative mycelium of monokaryotic *C. cinerea* strain Okayama 7 under nematode feeding pressure and the encoded proteins are toxic to different fungal foraging phyla [33, 34].

In our set up, induction of defense gene expression was most prominent for parts of the mycelium that were directly confronted with the nematode (Figure 1C). Within the confrontation area, the vast majority of hyphae expressed dTomato at high levels whereas in the control area, hyphae did not show any induction of the *cgl2p-dTom* reporter gene 18 – 24 h after addition of the nematodes (Figures 1C-D).

The local induction of defense genes after nematode foraging was also demonstrated for the second reporter strain, *C. cinerea* AmBm *cctx2p-dTom*, encoding the dTomato expression cassette under the control of the promoter for the chimerolectin CCTX2. Again, production of dTomato was only detected when nematodes were present and not in the control area (Figure S1C). Since the level of dTomato production observed in this strain was lower, compared to dTomato production driven by the *cgl2* promoter, further analyses of the *C. cinerea* defense response were carried out with the *C. cinerea* AmBm *cgl2p*-dTom strain.

A. avenae feeds by piercing the hyphal cell wall and ingesting the content of a hyphal compartment (Video S1). The active feeding by *A. avenae* seems to be required for the

induction of the *cgl2* promoter since the application of dead *A. avenae* did not, in accordance with previous results [33], trigger dTomato production in *C. cinerea* AmBm *cgl2p*-dTom (Figure S1C). Induction of dTomato was also not detected when, instead of *A. avenae,* bacteria (*B. subtilis* 168 and *E. coli* Nissle 1917) were applied to the confrontation area (Figure S1C).

The production of nematotoxic lectins, as observed by the production of dTomato, was detectable as early as approximately 6 h and became significant 18 h after the addition of *A. avenae* to the confrontation area (Figures 1D-E). Thus, the expression of defense effector genes was detected significantly earlier using the microfluidic FNI device than described previously (48h – 72h post nematode inoculation) [40]. qRT-PCR analysis of *C. cinerea* AmBm *cgl2p*-dTom hyphae collected from the confrontation area 6 h and 48 h post nematode application confirmed the differential expression of *cgl2* and *cctx2* (Figure 1E).

Propagation of defense response in trunk hyphae

The above analysis of *C. cinerea* AmBm *cgl2p-dTom* challenged with *A. avenae* showed that the induction of the *C. cinerea* anti-nematode defense response was primarily localized within the confrontation area and did not propagate systemically throughout the entire mycelium (e.g. into the control area harboring hyphae of the same colony, Figure 1C). However, detailed analysis of the acropetal and basipetal monitoring areas, where hyphae do not come into direct contact with *A. avenae*, revealed a systemic propagation of the induction in a distinct subset of hyphae. This systemic induction within individual hyphae was observed acropetally, as well as basipetally, originating from the confrontation area (Figures 2A-B). dTomato fluorescence within such hyphae was observed to spread over long distances, in some instances over several millimeters (> 2.5 mm). Importantly, the acropetal and basipetal transmission was not dependent on the promoter (*cgl2p*, *cctx2p* data not shown) or the fluorescent protein used (dTomato, eGFP) (Figure S1D). The speed of propagation of the fluorescence signal in both directions was similar and determined to be approximately 5 µm/sec. This value exceeds the apical growth rate of *C. cinerea* AmBm by a factor of about 75x (4.1 µm/min, [41]). The dTomato fluorescence signal rarely spread from an induced hypha into secondary branches, but was propagated from one hypha to another via anastomosis bridges (Figures S2A-B). Interestingly,

we could not detect any further propagation of the induction in the donor hyphae beyond the point of anastomosis.

Hyphae capable of long-distance propagation of the defense induction were otherwise not readily distinguishable from the rest of the hyphal population; however, the diameter of these hyphae appeared consistently large. We therefore analyzed the diameters of hyphae in the vegetative mycelium of *C. cinerea* AmBm. A two-step clustering analysis was performed and the results suggest that hyphae of a *C. cinerea* AmBm mycelium can be grouped into, on average, 2-3 distinct populations of hyphae based on the different hyphal diameters (Figures S2C-D). The average diameter of hyphae transmitting the dTomato fluorescence signal showed a mean diameter that clustered into the group of hyphae exhibiting a large diameter, here termed generally as trunk hyphae (Figure S2D) [13, 42].

Oscillation of defense response propagation

We followed the dTomato fluorescence in the trunk hyphae over time by acquiring a series of time-lapse images. The time-lapse series revealed that the fluorescence signal was propagated in the same hyphae several times within a 48 h time frame, seemingly switching between an on/off state in a regular fashion (Figure 2A). We analyzed the fluorescence intensity profiles (mean grey values) of a section in several induced hyphae over time and the analysis showed a periodicity of approximately 4-6 h for the individual hyphae between induced and non-induced states in both directions (as illustrated in Figures 2B-C, Video S2).

The dTomato-reporter protein was expressed as a cytosolic version that did not allow to differentiate between diffusion/transport of the dTomato protein from its expression site, and/or the diffusion/transport of the underlying fungal defense inducer from the confrontation area. To determine if the underlying fungal defense inducer is restricted to the site of nematode assault, we first constructed a *C. cinerea* AmBm reporter strain where dTomato localized to the nucleus. For this purpose, dTomato was fused to the *C. cinerea* histone H1 (*cgl2p*-dTomH1). When using this reporter strain, a fluorescence signal was observed in the nuclei of induced compartments and little to no dTomato was detected in the cytoplasm (Figures 2D-E). A detailed analysis of the co-cultivation between *A. avenae* and *C. cinerea* AmBm *cgl2p*-dTomH1 showed that the nuclear dTomato was still induced in distinct hyphae

within the acropetal and basipetal monitoring areas, which were not directly in contact with the nematode (Figure 2E). However, unlike in *C. cinerea* AmBm *cgl2p*-dTom, which expresses the cytosolic version of dTomato, induced hyphae in *C. cinerea* AmBm *cgl2p*-dTomH1 did not show any "on/off" state (Figure 2F). The fluorescence signal in the nuclei in these hyphae remained stable/increased over the measuring period.

Secondly, we tested the opening states of the dolipore septa in the acropetally and basipetally induced trunk hyphae. For this purpose, we performed fluorescence bleaching experiments since closed septa apparently represent a diffusion barrier for cytosolic dTomato in these hyphae (Figure S2A). The results indicate that, at the time of bleaching, not all septa along an induced hypha were open. The “-1 compartment” did not respond to the bleaching, indicating that the septa linking compartments 1 and -1 remained closed (Figures S3A–C). Furthermore, we observed that the opening state of a given septum can change over time. The septa connecting compartments 1 and -1 was closed at the time of the first bleaching, but opened 30 min later to allow transport of dTomato. The septa between compartment 3 and 4 on the other hand closed during the time course (Figures S3D-F).

Transport of nutrients in trunk hyphae

It is known that cord-forming basidiomycetes transport nutrients such as glucose or amino acids in a bidirectional manner and also show an oscillatory behavior [10, 20, 43]. Given the observed bidirectional propagation of the fungal defense response against nematodes within a specific subset of hyphae, we tested if the same hyphae were also used for transport of solutes within the mycelium. For this purpose, we employed the soluble and fluorescent glucose analog 2-NBDG. Instead of applying *A. avenae*, 30 µM of 2-NBDG was applied into the confrontation area and the fluorescence signal within the acropetal and basipetal monitoring areas was analyzed (Figure 3A). In contrast to the production of dTomato upon nematode challenge, distribution of 2-NBDG in the mycelium was far more complex. Septa of secondary or higher order branches were permeable to 2-NBDG, leading ultimately to diffusion of 2-NBDG throughout the mycelium (Figure 3B, ‘all hyphae’). Furthermore, 2-NBDG diffusion within the chamber itself was observed (Figure 3B, ‘background’). Nonetheless, we could clearly detect a fluorescence signal in some distinct hyphae

that exhibited a similar periodicity as those that had been induced by nematode challenge (Figures 3B; 'oscillatory hyphae'). These hyphae showed transport of 2-NBDG both acropetally and basipetally, approximately 1 h post application, whereas the arrival of 2-NBDG by general diffusion into the analyzed acropetal regions of interest (ROIs) was only apparent approximately 7 - 13 h post application and did not show a periodicity (Figure 3B, 'control hypha', 'all hyphae').

When *A. avenae* and 2-NBDG were added to the confrontation area at the same time, the dTomato and 2-NBDG fluorescence signals propagated along the same trunk hyphae with a synchronous oscillation (Figures S4A-G). Given the strikingly similar behavior observed for both molecules, we analyzed the time required for one periodic event (Figure 2C, Figure 3C) and found no statistical difference between dTomato and 2-NBDG or between acropetal and basipetal propagation (Figure S4H). To confirm a shared underlying distribution mechanism, we determined the theoretical concentration profile over time for dTomato (based on a 25kDa model protein) and 2-NBDG (based on diffusion kinetics of a typical ion) assuming distribution by simple diffusion only according to [24, 44] (Figures S5A, F).

The theoretical diffusion profile for dTomato is not in agreement with the fluorescence profile we obtained within propagating hyphae suggesting that simple diffusion over large distances (> 1000 μm) alone cannot account for the fast dTomato propagation kinetics observed (Figures S5B-E). Furthermore, the profile for 2-NBDG, while similar to the dTomato signal, also cannot be explained by a diffusion model, thus jointly suggesting a similar mechanism, different to diffusion, is underlying transport of these two molecules.

Finally, we asked whether an individual trunk hypha mediates transport both in the acropetal and basipetal directions to potentially explain the "on/off" state. We therefore introduced *A. avenae* into the confrontation area and 2-NBDG into the medium inlet (see Figures S1A-B for microfluidic device scheme). The results revealed that the defense response and 2-NBDG were still transported in the same hyphae, but that their transport was mutually exclusive and the oscillation of their transport was shifted by about half a period (2-3 h) (Figures 4A-G, Figure S4I).

Discussion

The present study reveals a yet undescribed functional differentiation of *C. cinerea* mycelia generating large trunk hyphae capable of bidirectional transport of bulk cytoplasmic solutes. This transport results in efficient distribution of nutrients and the systemic induction of defense genes, reaching a distance several millimeters from the actual site of predation.

Despite the broad versatility and variations in design, the application of microfluidic technology to study fungal growth and physiology or fungal interactions has only emerged in recent years [41, 45, 46]. The novel, tailor-made microfluidic device design presented here permitted the study of the dynamic interaction between the filamentous fungus *C. cinerea* and the fungivorous nematode *A. avenae* at the resolution of single hyphal compartments. In particular, the use of the FNI device to restrict the predatory nematode to specific mycelial areas, in combination with the use of fluorescent fungal reporter strains, made it possible to visualize the dynamic spatiotemporal distribution of the transcriptional response of the fungus to the nematode. It is anticipated that the set up and applications presented here, in particular the extraction of defined hyphal material, can be applied to many different physiological questions, where so far spatial resolution was lost due to the sampling technique employed.

The use of a fluorescent reporter strain in a microfluidic set up enabled us to follow the induction of defense genes of this fungus to nematode predation in real-time and with single cell resolution. Our results show that different parts of a basidiomycete mycelium are autonomous in their response to environmental stimuli, as the defense response was only elicited in areas directly confronted with the nematode (Figure 1C). Differences in gene expression and protein secretion between different hyphae of a mycelial colony were previously demonstrated for *Aspergillus niger* [56-58]. In contrast to *C. cinerea*, however, the observed gene expression differences within the *A. niger* mycelium were constitutive and not induced by external cues.

The strong response of the *C. cinerea* hyphae to *A. avenae* in the confrontation area of the microfluidic device allowed us to probe the specificity of this defense response (Figure S1C). Our observations confirmed previous results suggesting that inducible fungal defense is very specific for the respective antagonist and that the anti-nematode response relies on active feeding by the nematode [33, 34]. The time

required to induce the anti-nematode response within the mycelium is comparable to the induction of plant defense against herbivory (Figures 1D, E) [47]. The fact that two different defense effector promotors (*cgl2p* and *cctx2p*) were activated with similar kinetics suggests that both promoters could be activated by the same signal transduction pathway. The nature of the nematode signal perceived by the fungus, the mode of signal recognition or the components of the signal transduction pathways, however, remain to be elucidated.

In a subset of hyphae, characterized by their large diameter and referred to as trunk hyphae, the induction of the defense gene promotor was not limited to the site of predation, but was propagated over several millimeters (Figure 2). Interestingly, this propagation occurred not only in the growth direction (acropetal) but also in basipetal direction from the confrontation area (Figure 2A). The nuclearly targeted version of the dTomato reporter protein (*cgl2p*-dTom-H1) still showed acropetal and basipetal propagation along this subset of hyphae, indicating that, besides cytosolic dTomato, also the underlying inducer of the defense effector-encoding genes is transported. Since fluorescence of this nuclearly targeted version of dTomato did not, in contrast to the cytosolic dTomato, show any "on/off" state (Figures 2A, F), we hypothesize that oscillation of the cytosolic dTomato version is based on cytoplasmic flow.

The concept of acropetal and basipetal cytoplasmic flows within a fungal colony is not new. Previous studies demonstrated bidirectional nutrient translocation within cords or rhizomorphs of saprophytic and ectomycorrhizal basidiomycetes [8, 10, 20, 23, 43, 48, 49]. Bidirectionality was explained to be due to dedicated acro- and basipetally oriented, hyphal bundles within cords or rhizomorphs. The use of periodic cytoplasmic flows to increase the dispersion of a molecule was also described for the network of syncytical veins in the slime mold *Physarum polycepharum* [49, 50]. Tlalka *et al.* showed for the first time that N-transport (2 Aminoisobutyric acid, ^{14}C-AIB) within cords of *Phaenerochate velutina* underlies a certain periodicity which was dependent on the subdomain of mycelium observed [51]. However, while transport of ^{14}C-AIB in *P. velutina* followed a pulsatile behavior with an oscillatory rhythm of around 11 - 14 h [20, 51], the length of oscillation observed in our experiments were shorter (4-6 h) and hyphal bundles or cords are not present in the vegetative mycelium of *C. cinerea* [52]. Instead we could identify, using the novel microfluidic setup, a distinct subtype of individual hyphae, morphologically only

distinguishable by their large diameter, that was responsible for the transport (Figures S2C-D).

In accordance with the cytoplasmic transport hypothesis for the observed phenomena with the fluorescent defense reporter strain, the application of a fluorescent glucose analog, 2-NBDG, used previously for the characterization of solute transport in hyphae of the ascomycete *Aspergillus niger* [53], to the *C. cinerea* mycelium, either independently or concomitantly with the nematode, revealed transport along the same hyphae with similar kinetics and periodicity as the dTomato fluorescence signal (Figure 3; Figures S4A-H). In addition, we find that neither the dTomato nor the 2-NBDG fluorescence signal propagation correlate with their respective expected diffusion kinetics (Figure S5).

Taken together, these results suggest the presence of a bulk transport of solutes within the *C. cinerea* mycelium, both in acropetal and basipetal direction that covers distances beyond the dimensions of our microfluidic devices (3.5 mm) and may allow a fast and efficient distribution of nutrients and signals (Figure 5, Figure S5). In contrast to previous reports on other basidiomycetes, this bidirectional transport in *C. cinerea* appears to occur at the level of individual hypha rather than bundles of hyphae (Figure 4). We speculate that the oscillation, observed for transport of both dTomato and 2-NBDG (Figure 2, Figure 3), is caused by periodical (every 2-3 h) switching of the direction of bulk transport in these hyphae. Such a distribution mechanism of solutes would, on the one hand, equilibrate fluctuations and imbalances of individual nutrients between distant areas of the mycelium and ensure mycelial growth in environments where nutrients are distributed unevenly [12, 18, 49, 50]. On the other hand, the fast transmission of signals inducing anti-predator defense in areas of the mycelium that are not yet under attack might save vital parts of the mycelium from predator damage and thus ensure survival of the organism as shown for plants [47]. This type of organismic defense is possible due to the ability of fungal mycelia to survive, even if large parts thereof are destroyed, and to regenerate from the remaining parts [35, 36].

At present, we can only speculate how the detected specialized transport hyphae in the vegetative mycelium of *C. cinerea* generate their cytoplasmic flow and periodically change its direction. Fluorescence bleaching and recovery experiments on induced hyphal compartments – outside of the confrontation area – indicate that the opening state of the septal pores in the propagating hyphae is reversible and that

cytoplasmic continuity can be interrupted at a given time (Figure S3). We hypothesize that the coordinated, reversible closure of the septal pores is a major factor in the bidirectional transport in these hyphae. The generation of such flows allows a faster and more efficient redistribution of nutrients and signals within the hyphal colony as compared to simple diffusion (Figures 3-5, S4, S5) [24]. It remains to be elucidated as to why and how hyphal branches are connected and disconnected from this transport system.

In summary, the study of inducible defense against fungivorous nematodes in the basidiomycete *C. cinerea* has revealed a novel type of hyphal differentiation and communication within a fungal mycelium and the next challenge will be to unravel the molecular mechanisms responsible for these phenomena.

Acknowledgements

Access to the Zeiss LSM780 was kindly provided by the Scientific Center for Optical and Electron Microscopy (ScopeM). This work was supported by the Swiss National Science Foundation (No. 31003A_130671 to M.K. and PZ00P2_168005 to C.E.S) and ETH Zürich.

Author contributions

Conceptualization, M.K.; Methodology, S.S., C.E.S., D.vS, J.S., A.R., S.N.; Investigation, S.S., C.E.S.; Formal Analysis, S.S., C.E.S., A.R., S.N.; Writing – Original Draft, S.S., C.E.S., M.K.; Writing – Review & Editing, S.S., C.E.S., M.K., A.R.; Visualization, S.S., C.E.S.; Supervision, M.K., M.A., A.dM; Funding Acquisition, M.K.

Declaration of interests

The authors declare no competing interests.

References

1. Hutchings, M., Wijesinghe, D., and John, E. (2000). The effects of heterogeneous nutrient supply on plant performance: a survey of responses, with special reference to clonal herbs. The ecological consequences of environmental heterogeneity, 91-110.
2. Burnett, J.H. (2003). Fungal populations and species, (Oxford University Press).
3. Rayner, A., Griffith, G., and Ainsworth, A. (1995). Mycelial interconnectedness. In The growing fungus. (Springer), pp. 21-40.
4. Prosser, J.I., and Trinci, A.P. (1979). A model for hyphal growth and branching. J Gen Microbiol *111*, 153-164.
5. Glass, N.L., Rasmussen, C., Roca, M.G., and Read, N.D. (2004). Hyphal homing, fusion and mycelial interconnectedness. Trends Microbiol *12*, 135-141.
6. Glass, N.L., Jacobson, D.J., and Shiu, P.K. (2000). The genetics of hyphal fusion and vegetative incompatibility in filamentous ascomycete fungi. Annu Rev Genet *34*, 165-186.
7. Carlile, M.J., Watkinson, S.C., and Gooday, G.W. (2001). The fungi, 2nd Edition, (London and San Diego: Academic Press).
8. Boddy, L. (1999). Saprotrophic cord-forming fungi: meeting the challenge of heterogeneous environments. Mycologia *91*, 13-32.
9. Fricker, M.D., Lee, J.A., Bebber, D.P., Tlalka, M., Hynes, J., Darrah, P.R., Watkinson, S.C., and Boddy, L. (2008). Imaging complex nutrient dynamics in mycelial networks. J Microsc *231*, 317-331.
10. Fricker, M.D., Tlalka, M., Bebber, D., Takagi, S., Watkinson, S.C., and Darrah, P.R. (2007). Fourier-based spatial mapping of oscillatory phenomena in fungi. Fungal Genet Biol *44*, 1077-1084.
11. Davidson, F.A., and Olsson, S. (2000). Translocation induced outgrowth of fungi in nutrient-free environments. J Theor Biol *205*, 73-84.
12. Olsson, S. (2001). Colonial Growth of Fungi. In Biology of the Fungal Cell, Volume 8, R. Howard and N.R. Gow, eds. (Springer Berlin Heidelberg), pp. 125-141.
13. Simonin, A., Palma-Guerrero, J., Fricker, M., and Glass, N.L. (2012). Physiological significance of network organization in fungi. Eukaryot Cell *11*, 1345-1352.
14. Cairney, J.W. (2005). Basidiomycete mycelia in forest soils: dimensions, dynamics and roles in nutrient distribution. Mycol Res *109*, 7-20.
15. Bebber, D.P., Hynes, J., Darrah, P.R., Boddy, L., and Fricker, M.D. (2007). Biological solutions to transport network design. Proc Biol Sci *274*, 2307-2315.
16. Agerer, R. (2001). Exploration types of ectomycorrhizae - A proposal to classify ectomycorrhizal mycelial systems according to their patterns of differentiation and putative ecological importance. Mycorrhiza *11*, 107-114.
17. Genney, D.R., Anderson, I.C., and Alexander, I.J. (2006). Fine-scale distribution of pine ectomycorrhizas and their extramatrical mycelium. New Phytologist *170*, 381-390.
18. Tlalka, M., Bebber, D., Darrah, P.R., and Watkinson, S.C. (2008). Mycelial networks: nutrient uptake, translocation and role in ecosystems. In British Mycological Society Symposia Series, Volume 28. (Elsevier), pp. 43-62.
19. Watkinson, S.C., Boddy, L., Burton, K., Darrah, P., Eastwood, D., Fricker, M.D., and Tlalka, M. (2005). New approaches to investigating the function of mycelial networks. Mycologist *19*, 11-17.

20. Tlalka, M., Bebber, D.P., Darrah, P.R., Watkinson, S.C., and Fricker, M.D. (2008). Quantifying dynamic resource allocation illuminates foraging strategy in Phanerochaete velutina. Fungal Genet Biol *45*, 1111-1121.
21. Lew, R.R. (2011). How does a hypha grow? The biophysics of pressurized growth in fungi. Nature Reviews Microbiology *9*, 509-518.
22. Heaton, L., Obara, B., Grau, V., Jones, N., Nakagaki, T., Boddy, L., and Fricker, M.D. (2012). Analysis of fungal networks. Fungal Biology Reviews *26*, 12-29.
23. Olsson, S., and Gray, S.N. (1998). Patterns and dynamics of 32P-phosphate and labelled 2-aminoisobutyric acid (14C-AIB) translocation in intact basidiomycete mycelia. FEMS Microbiology Ecology *26*, 109-120.
24. Fricker, M.D., Heaton, L.L.M., Jones, N.S., and Boddy, L. (2017). The Mycelium as a Network. Microbiol Spectr *5*.
25. Spiteller, P. (2008). Chemical defence strategies of higher fungi.
26. Rohlfs, M., and Churchill, A.C.L. (2011). Fungal secondary metabolites as modulators of interactions with insects and other arthropods. Fungal Genet Biol *48*, 23-34.
27. Stadler, M., and Sterner, O. (1998). Production of bioactive secondary metabolites in the fruit bodies of macrofungi as a response to injury. Phytochemistry *49*, 1013-1019.
28. Sabotic, J., Ohm, R.A., and Kunzler, M. (2016). Entomotoxic and nematotoxic lectins and protease inhibitors from fungal fruiting bodies. Appl Microbiol Biotechnol *100*, 91-111.
29. Wang, M., Trigueros, V., Paquereau, L., Chavant, L., and Fournier, D. (2002). Proteins as active compounds involved in insecticidal activity of mushroom fruitbodies. J Econ Entomol *95*, 603-607.
30. Nützmann, H.-W., Reyes-Dominguez, Y., Scherlach, K., Schroeckh, V., Horn, F., Gacek, A., Schümann, J., Hertweck, C., Strauss, J., and Brakhage, A.A. (2011). Bacteria-induced natural product formation in the fungus Aspergillus nidulans requires Saga/Ada-mediated histone acetylation. Proceedings of the National Academy of Sciences *108*, 14282-14287.
31. Park, H.B., Kwon, H.C., Lee, C.-H., and Yang, H.O. (2009). Glionitrin A, an antibiotic– antitumor metabolite derived from competitive interaction between abandoned mine microbes. Journal of natural products *72*, 248-252.
32. Brandt, P., Garcia-Altares, M., Nett, M., Hertweck, C., and Hoffmeister, D. (2017). Induced Chemical Defense of a Mushroom by a Double-Bond-Shifting Polyene Synthase. Angew Chem Int Ed Engl.
33. Bleuler-Martinez, S., Butschi, A., Garbani, M., Walti, M.A., Wohlschlager, T., Potthoff, E., Sabotic, J., Pohleven, J., Luthy, P., Hengartner, M.O., et al. (2011). A lectin-mediated resistance of higher fungi against predators and parasites. Mol Ecol *20*, 3056-3070.
34. Plaza, D.F., Schmieder, S.S., Lipzen, A., Lindquist, E., and Künzler, M. (2016). Identification of a Novel Nematotoxic Protein by Challenging the Model Mushroom Coprinopsis cinerea with a Fungivorous Nematode. G3: Genes| Genomes| Genetics *6*, 87-98.
35. Crowther, T.W., Boddy, L., and Hefin Jones, T. (2012). Functional and ecological consequences of saprotrophic fungus-grazer interactions. ISME J *6*, 1992-2001.
36. Crowther, T.W., and A'Bear, A.D. (2012). Impacts of grazing soil fauna on decomposer fungi are species-specific and density-dependent. Fungal Ecology *5*, 277-281.

37. Boddy, L., Wood, J., Redman, E., Hynes, J., and Fricker, M.D. (2010). Fungal network responses to grazing. Fungal Genet Biol *47*, 522-530.
38. Stanley, C.E., Grossmann, G., i Solvas, X.C., and deMello, A.J. (2016). Soil-on-a-Chip: microfluidic platforms for environmental organismal studies. Lab Chip *16*, 228-241.
39. Stanley, C.E., Stockli, M., van Swaay, D., Sabotic, J., Kallio, P.T., Kunzler, M., deMello, A.J., and Aebi, M. (2014). Probing bacterial-fungal interactions at the single cell level. Integr Biol (Camb) *6*, 935-945.
40. Plaza, D.F., Schmieder, S.S., Lipzen, A., Lindquist, E., and Kunzler, M. (2015). Identification of a Novel Nematotoxic Protein by Challenging the Model Mushroom Coprinopsis cinerea with a Fungivorous Nematode. G3 (Bethesda) *6*, 87-98.
41. Stanley, C.E., Stöckli, M., van Swaay, D., Sabotič, J., Kallio, P.T., Künzler, M., and Aebi, M. (2014). Probing bacterial–fungal interactions at the single cell level. Integrative Biology *6*, 935-945.
42. N. Bistis, G., D. Perkins, D., and Read, N. (2003). Different cell types in Neurospora crassa, Volume 50.
43. Lindahl, B., Finlay, R., and Olsson, S. (2001). Simultaneous, bidirectional translocation of 32P and 33P between wood blocks connected by mycelial cords of Hypholoma fasciculare. New Phytologist *150*, 189-194.
44. Cushman-Roisin, B. (2012). ENGS 43: Environmental Transport and Fate; Chapter 2. .
45. Held, M., Edwards, C., and Nicolau, D.V. (2011). Probing the growth dynamics of Neurospora crassa with microfluidic structures. Fungal Biol *115*, 493-505.
46. Hanson, K.L., Nicolau, D.V., Filipponi, L., Wang, L.S., Lee, A.P., and Nicolau, D.V. (2006). Fungi use efficient algorithms for the exploration of microfluidic networks. Small *2*, 1212-1220.
47. Toyota, M., Spencer, D., Sawai-Toyota, S., Jiaqi, W., Zhang, T., Koo, A.J., Howe, G.A., and Gilroy, S. (2018). Glutamate triggers long-distance, calcium-based plant defense signaling. Science *361*, 1112-1115.
48. Cairney, J.W.G. (1992). Translocation of Solutes in Ectomycorrhizal and Saprotrophic Rhizomorphs. Mycological Research *96*, 135-141.
49. Alim, K., Andrew, N., Pringle, A., and Brenner, M.P. (2017). Mechanism of signal propagation in Physarum polycephalum. Proceedings of the National Academy of Sciences of the United States of America *114*, 5136-5141.
50. Marbach, S., Alim, K., Andrew, N., Pringle, A., and Brenner, M.P. (2016). Pruning to Increase Taylor Dispersion in Physarum polycephalum Networks. Phys Rev Lett *117*, 178103.
51. Tlalka, M., Bebber, D.P., Darrah, P.R., Watkinson, S.C., and Fricker, M.D. (2007). Emergence of self-organised oscillatory domains in fungal mycelia. Fungal Genet Biol *44*, 1085-1095.
52. Kues, U. (2000). Life history and developmental processes in the basidiomycete Coprinus cinereus. Microbiol Mol Biol Rev *64*, 316-353.
53. Bleichrodt, R.J., Vinck, A., Read, N.D., and Wosten, H.A.B. (2015). Selective transport between heterogeneous hyphal compartments via the plasma membrane lining septal walls of Aspergillus niger. Fungal Genet Biol *82*, 193-200.
54. Staniland, L.N. (1954). A modification of the Baermann funnel technique for the collection of nematodes from plant material. J Helminthol *28*, 115-117.
55. Walti, M.A., Villalba, C., Buser, R.M., Grunler, A., Aebi, M., and Kunzler, M. (2006). Targeted gene silencing in the model mushroom Coprinopsis cinerea

(Coprinus cinereus) by expression of homologous hairpin RNAs. Eukaryot Cell *5*, 732-744.

56. Schindelin, J., Arganda-Carreras, I., Frise, E., Kaynig, V., Longair, M., Pietzsch, T., Preibisch, S., Rueden, C., Saalfeld, S., Schmid, B., et al. (2012). Fiji: an open-source platform for biological-image analysis. Nature methods *9*, 676-682.

57. Plaza, D.F., Lin, C.W., van der Velden, N.S., Aebi, M., and Kunzler, M. (2014). Comparative transcriptomics of the model mushroom Coprinopsis cinerea reveals tissue-specific armories and a conserved circuitry for sexual development. BMC Genomics *15*, 492.

Figure titles and legends

Figure 1. Local induction of the *cgl2* promoter in *C. cinerea* mycelium upon nematode predation. (A) Design of the Fungal-Nematode-Interaction (FNI) microfluidic device. Scheme shows a two-dimensional overview of the microchannel geometry used to accommodate the fungal hyphae, originating from the inoculum, and inlets used for the application of nematodes (confrontation area with parallel control area) or solutes (medium inlet). The height of the microchannels within the entire device is 10 µm. Scale bar = 500 µm. (B) Photograph of the FNI microfluidic device. In the example shown, the device was inoculated with *C. cinerea* on YMG agar and incubated for 18 h at 37 °C. Scale bar = 5 mm. (C) Tiled bright field and fluorescent image of the control and confrontation area of a FNI microfluidic device containing *C. cinerea* strain AmBm *cgl2p-dTom* 16 h post-co-inoculation with the fungivorous nematode *A. avenae*. Production of dTomato driven by the *cgl2* promoter was only visible in the confrontation but not in the control area. Images represent the monitoring areas depicted by the red boxes in panel (A). Scale bar = 100 µm. (D) Quantification of dTomato production in the confrontation area over a 24 h time course post-co-inoculation of *A. avenae*. Relative fluorescence (mean grey values) of ¼ of the confrontation and control area (24h ctrl) for six biological replicates are plotted. The 18 h time point and 24 h time point are statistically significantly different to the 24 h control time point. A one-way ANOVA and Kruskal-Wallis test was performed. The asterisk (*) indicates a p-value < 0.05, whereas (**) indicates a p-value < 0.01. AU = arbitrary units. Error bars indicate standard deviations. (E) qRT-PCR analysis of the nematode induction of the *cgl2* and *cctx2* genes in *C. cinerea* AmBm *cgl2p-dTom* using material extracted from the confrontation/control area in the FNI microfluidic device at two different time points post-co-inoculation with *A. avenae*. Bars represent the mean $\log_2$ fold changes of the expression of the defense genes between confrontation and control area among three replicates. Error bars indicate standard deviations. See also Figure S1 and Video S1.

Figure 2. Acropetal and basipetal propagation of *cgl2p-dTom* induction in specialized hyphae. (A) *A. avenae* was introduced into the confrontation area of a microfluidic device containing the *C. cinerea* AmBm *cgl2p-dTom* reporter strain 16 h prior to image acquisition. After this preincubation period, a time-lapse image series

with a 30 min interval between frames was recorded. Arrowheads indicate the monitored hyphae and the location for the fluorescence intensity measurement. Representative images for acropetal and basipetal propagation are shown. Scale bar = 100 µm. (B) Analysis of fluorescence mean grey values for hyphae in (A) over all time points for the acropetal and basipetal monitoring areas. Dashed lines indicate the time points represented in (A). (C) Comparison of the oscillation periods of dTomato propagation in acropetal (AP) and basipetal (BP) direction. The periods were measured in at least eight independent experiments, with a maximum of two analyzed hyphae per experiment. Mann-Whitney test was employed to assess statistical difference between AP and BP mean oscillation periods. Error bars indicate standard deviations. (D) Propagation of the production of *cgl2p*-driven dTom-H1 fusion protein. *A. avenae* was introduced into the confrontation area of a microfluidic device containing the *C. cinerea* AmBm *cgl2p-dTom-H1* reporter strain 16 h prior to monitoring the fluorescence intensity. Activation of *cgl2p* leads to the production of nuclearly localized dTomato-H1 fusion protein in the induced hyphae. Inset shows the extent of nuclear localization. Scale bar = 100 µm. (E) Individually induced hyphae (indicated with arrowheads) can be observed in the acropetal and basipetal monitoring areas. Scale bar = 30 µm. (F) Fluorescence profile over time for representative nuclei. Upper left panel shows an overview of basipetal monitoring area. Six nuclei in the basipetal monitoring area, indicated by the arrowheads, were chosen for the analysis. All six nuclei stem from different individual hyphae. Upper right panels show representative images taken from the time series of nucleus number two. Scale bars = 100 µm and 10 µm respectively. Lower panel shows the change in fluorescence mean grey values of the six nuclei, shown in the overview, over time. See also Figure S2, Figure S3 and Video S2.

Figure 3. 2-NBDG transport in *C. cinerea* mycelium. 30 µM of 2-NBDG was added to the confrontation area and a time-lapse image series was acquired to track the distribution of 2-NBDG within the mycelium. A 15 min or 30 min time interval between frames was used for the acropetal and basipetal monitoring areas, respectively. (A) Left: overview of an acropetal and basipetal monitoring area of two independent devices. Right panels show representative images taken from the time series of individual oscillating hypha (indicated by arrowheads) for the insets marked in the respective overview. Scale bars = 100 µm (overview) and 20 µm (time series).

(B) Graph showing the mean grey values over time for four hyphae, where an oscillating 2-NBDG fluorescence signal was apparent (Osc. hyphae 1-4: green circles). The background fluorescence intensity in these regions increased over time without showing any periodicity (Background: filled black square). This is also true for individual non-oscillating hyphae (Ctrl. hypha: black open diamond), and for the total fluorescence intensity of all hyphae (all hyphae: black closed triangle). The dashed lines indicate the time points depicted in the time series. (C) Comparison of the oscillation periods of 2-NBDG propagation in acropetal (AP) and basipetal (BP) direction. The periods were measured in at least eight independent experiments, with a maximum of two hyphae per experiment. Mann-Whitney test was performed to test for statistical significance. Error bars indicate standard deviations. See also Figures S4.

Figure 4. Bidirectional and antiphase propagation of *cgl2p-dTom* induction and 2-NBDG within the same hypha. *A. avenae* was added into the confrontation area 24 h prior to the addition of 30 µM 2-NBDG to the medium inlet of a FNI microfluidic device containing the *C. cinerea* AmBm *cgl2p-dTom* reporter strain. A time-lapse study was performed to determine whether acropetal and basipetal propagation of fluorescence occur simultaneous within the same hyphae. (A) Left: overview of the 2-NBDG fluorescence intensity ca. 3 h post addition of 2-NBDG to the medium inlet. Two regions of interest comprising exemplary propagating hyphae were selected and monitored for both dTomato and 2-NBDG fluorescence over time. The images were false coloured using the inverted Green FIRE blue LUT (2-NBDG) and the inverted FIRE LUT (dTomato). Right panels show representative images taken from the time series of the frames 1 and 2. Arrowheads indicate the hyphae monitored and the positions at which quantification in (B) was performed. Scale bars = 100 µm (overview) and 20 µm (time series). (B) Graph showing the relative dTomato and 2-NBDG fluorescence intensities of the selected hyphae in the acropetal monitoring area over time. The dTomato fluorescence intensity values were shifted by 0.05 AU for visualization (see Star Methods). The dashed lines indicate the time points shown in panel (A). (C) Kymograph spanning the length of the two hyphae of interest in (A) and (B) and a control (non-oscillating) hypha, note the increase in 2-NBDG fluorescence over time for the control hypha, absent for the oscillating hyphae. Hyphae were traced in growth direction over the

whole field of view and fluorescence intensity is plotted over time. (D) Overlay of the oscillation behavior shown in (B) after spatial averaging and detrending. The signal-to-noise ratio of the time series was improved using spatial and temporal averaging with 7x7 and 5x5 pixel kernel and the data was detrended with rolling average of 30 prior to smoothing with a Hanning window. (E) Graph as in (B) for two additional hyphae, of a different ROI, showing the relative dTomato and 2-NBDG fluorescence intensities in the acropetal monitoring area over time. (F) Kymograph as in (C) for the two hyphae of interest in (E) and a control (non-oscillating) hypha, note the increase in 2-NBDG fluorescence over time for the control hypha, absent for the oscillating hyphae. (G) Overlay of the oscillation behavior shown in (E) after spatial averaging and detrending performed as in (D). See also Figures S4 and S5.

Figure 5. Model for long-distance propagation of gene expression patterns and the distribution of nutrients within trunk hyphae of *C. cinerea*. Based on the data presented in this study, we propose that a distinct subset of hyphae (trunk hyphae) in the *C. cinerea* AmutBmut mycelium possesses the ability to alternate the direction of their cytoplasmic bulk mass flow periodically (every 2-3 h). In the basipetal flow mode, the septa along the trunk hypha, including the ones towards the branches, are open to allow distribution of nutrients (2-NBDG) absorbed at the hyphal tips to subapical regions of the mycelium. Similarly, nematode assault leads to the induction of defense gene expression and the propagation of this expression pattern (most likely by bulk flow transport of an internal signal molecule) in basipetal direction. In the acropetal flow mode, the septa along the trunk hypha are open while the septa towards the branches are closed, channeling the propagation of signals and the distribution of nutrients in the (acropetal) direction of hyphal growth. The underlying molecular mechanisms that govern this behavior are unknown. Arrows indicate direction of flow. Red filling represents induction of cytoplasmic dTomato expression in response to predation by nematodes (indicated by a schematic representation of their heads and stylets), whereas green hexagons within the hyphae represent nutrients (2-NBDG). See also Figures S3-S5.

STAR*METHODS

Detailed methods are provided in the online version of this paper and include the following:

KEY RESOURCES TABLE

CONTACT FOR REAGENT AND RESOURCE SHARING

Further information and requests for resources and reagents should be directed to and will be fulfilled by the Lead Contact, Markus Künzler (mkuenzle@ethz.ch).

EXPERIMENTAL MODELS AND SUBJECT DETAILS

Strains and general cultivation conditions

All organisms and strains used in this study are summarized in Table S1. Information on growth media and antibiotics can be found in the Key Resource table. *Escherichia coli* DH5α was used for cloning and amplification of pRS426-derived plasmids and cultivated on Luria Bertani (LB) medium supplemented with 100 µg/ml ampicillin. *Escherichia coli* Nissle 1917 and *Bacillus subtilis* 168 were used to challenge the *Coprinopsis cinerea* reporter strains and both were grown in LB broth at 37 °C [34]. *Saccharomyces cerevisiae* laboratory strain W303 (*MATa ade2-1 leu2-3,112 his3-11,15 ura3-1 can1-100 trp1-1*) was used for homologous recombination of plasmids and cultivated on YPD medium at 30 °C as described [41]. Transformants were selected on SD medium without uracil.

Vegetative mycelium of *C. cinerea* strain A43mutB43mut (AmBm; homodikaryon) and the respective transformants were generally cultivated on YMG agar plates at 37 °C in the dark. The fungivorous nematode *Aphelenchus avenae* (a kind gift from Prof. Richard Sikora, University of Bonn, Germany) was propagated at 20 °C on vegetative mycelium of *Agaricus bisporus* pre-grown on PDA plates (Difco). Nematode harvesting was conducted using the Baermann funnel method [54]. In brief, a funnel was laid out with tissue paper to retain fungal and plate material and the bottom part was wrapped with aluminum foil. The fungal-nematode co-culture was then submerged into the water-filled funnel. After 12 h the nematodes were collected by drawing the bottom 2 cm of water. After harvesting, nematodes were transferred to water agar plates supplemented with 200 µg/mL G418, 50 µg/mL Nystatin and 100 µg/mL Ampicillin, and incubated for 48 h to eliminate all residual fungal

744 contamination. *C. cinerea* AmBm - *A. avenae* co-cultivations were incubated at 20 °C
745 in the dark for the time indicated.

746

747 **METHOD DETAILS**

748 **Generation of *C. cinerea* reporter strains**

749 All plasmids used and generated in this study are listed in Table S1. All primer
750 sequences can be found in Table S2. Plasmid pMA541, coding for a *cgl2p-dTomato*
751 reporter gene in *C. cinerea,* was generated using pMA412, which encodes a dTomato
752 expression cassette driven by the *A. bisporus gpdII* promoter and containing a *pab1*
753 selection marker for *C. cinerea* in the vector backbone [39]. The *A. bisporus gpdII*
754 promoter was replaced by the *C. cinerea cgl2* promoter (*cgl2p*). The *C. cinerea cgl2*
755 promoter was amplified from genomic DNA with flanking homology regions for
756 recombination into pMA412 (for primer sequences see Table S2). Homologous
757 recombination of *Cla*I-*Xho*I opened pMA412 and the PCR-generated *cgl2p*-fragment
758 was performed in *S. cerevisiae* W303. Selection of positive clones was done on SD
759 medium without uracil [55]. Correct exchange of the *A. bisporus gpdII* promoter by
760 the *C. cinerea cgl2* promoter resulting in plasmid pMA541 was confirmed by
761 sequencing (Microsynth, Switzerland). Transformation of *C. cinerea* AmBm with
762 pMA541 was carried out by protoplasting oidia as described previously [41, 55].
763 Nuclear localization of dTomato was achieved by fusing the coding region for
764 dTomato to the one for histone H1 from *C. cinerea* (JGI Protein ID 467558) to create
765 a H1-dTomato fusion protein. The plasmid pMA1130 was generated by amplifying the
766 complete 467558 coding region (including introns) from genomic DNA with
767 corresponding flanking homology regions for homologous integration into pMA541.
768 pMA541 was linearized using the restriction enzyme *Fsp*AI (Thermo Scientific,
769 California, USA).

770 Plasmid pMA1101 was generated in the same manner as pMA541 but amplifying the
771 *cctx2* promoter region with corresponding flanking regions for recombination into
772 pMA412 [34]. For pMA1131, the dTomato expression cassette in pMA541 was
773 exchanged for an eGFP cassette with the intron-exon structure of the *cgl2* locus.
774 Latter cassette was amplified from plasmid 341 (pRS426-benA-cgl2::eGFP) [55] with
775 the respective flanking homology regions for integration into pMA541. Plasmid

776 pMA541 was linearized using *Bsr*GI for this purpose. Homologous recombination as
777 well as transformation into *C. cinerea* AmBm was performed as described above.

778

779 **Microfluidic device design and manufacturing**

780 Microfluidic devices were prepared as described in Stanley *et al.* [41]. In brief: Master
781 moulds were manufactured using a polyester film photolithography mask (Micro
782 Lithography Services Ltd. UK) and a 100 mm silicon wafer (Silicon Materials,
783 Germany) spin-coated with SU-8 photoresist (MicroChem, USA) aiming for a target
784 height of 10 µm. Poly(dimethylsiloxane) (PDMS) silicone elastomer was prepared
785 using a 10:1 ratio of base to curing agent (Sylgard 184, Dow Corning, USA) that was
786 thoroughly mixed, degassed and then poured onto the master mould. After curing
787 overnight at 70 °C, the PDMS was removed from the mould and diced into slabs. A
788 precision cutter (Syneo, USA), having a cutting edge diameter of 3.02 mm, was used
789 to punch the holes for the medium inlet. The control and confrontation areas were
790 always kept consistent between experiments, each corresponding to an area of ca. 5
791 mm^2 (Figures 1A-B, Figures S1A-B). Precision cutters with a cutting edge diameter of
792 1.65 or 2.49 mm were used to create the control/confrontation areas.

793 PDMS slabs and glass-bottomed Petri dishes (World Precision Instruments) were
794 washed in 0.5 M sodium hydroxide (Sigma-Aldrich, Germany), 70 % v/v ethanol, and
795 sterile double distilled water (ddH2O). The PDMS slabs and Petri dishes were then
796 dried at 70 °C for 1 h, bonded and filled with sterile-filtered yeast maltose glucose
797 (YMG) medium.

798

799 **Imaging of fungal-nematode co-cultures**

800 The respective *C. cinerea* strain was cultivated at 37 °C in a dark, humid box for 72 h.
801 Inoculation of a YMG-filled microfluidic device was performed as described in
802 Stanley *et al.* [41] with the following modification: the inoculated microfluidic device
803 was incubated in the dark with high humidity for approximately 18 h at 37 °C to allow
804 the hyphae to grow into the confrontation and control areas (Figures 1A-B, S1A-B)
805 before the addition of nematodes. For every experiment, approx. 5 nematodes of a
806 mixed stage population were transferred into the inlet that leads to the confrontation

area. Following the addition of nematodes, the co-cultivation devices were monitored immediately or transferred to 20 °C in the dark for later use.

Image acquisition was performed as described in Stanley *et al.* [41]. In brief, a Nikon Ti-U inverted widefield fluorescence microscope, was used for long-term, time-lapse experiments. The microscope was equipped with a Prior ProScan III motorized stage (Prior Scientific, UK) and a CoolSNAP HQ2 camera (Photometrics, Germany). Bright field images were acquired with using phase contrast microscopy with a ×20/0.45 NA S Plan Fluor objective lens (Nikon, Switzerland), and 100 ms exposure time.

Epifluorescence images were captured using a Nikon Intensilight C-HGFI mercury lamp (Nikon, Switzerland) as the source of excitation. TRITC and FITC HC BrightLine Basic Filtersets (AHF Analysentechnik, Germany) were used to image dTomato expression and the fluorescent glucose analog 2-NBDG (Life technologies) respectively (with exposure times of 100 and 200 ms respectively). Imaging experiments were coordinated with NIS-Elements Advanced Research imaging software (Nikon, Switzerland) and performed in a temperature controlled dark room at 20 °C.

Images were analyzed using open software Fiji [56]. To measure the hyphal diameter the free hand tool and measuring tool of Fiji were used. The measuring tool was also used to analyze grey values.

QUANTIFICATION AND STATISTICAL ANALYSIS

Validation of defense gene expression

To validate the expression levels of the nematotoxin-encoding *C. cinerea* genes *cgl2* and *cctx2*, hyphal material was extracted from the confrontation area after 6 and 48 h and flash frozen in liquid nitrogen. Hyphae were lysed using glass beads, as described previously [34, 57]. Total RNA was extracted using a PicoPure RNA isolation kit (Life Technologies, California, USA). The quality of the extracted RNA was controlled using a Bioanalyzer 2100 (Agilent). Quantitative real-time polymerase chain reaction (qRT-PCR) for the individual defense genes was carried out according to Plaza *et al.* [34]. In brief, single-stranded cDNA was synthesized using Transcriptor Universal cDNA Master (Roche). qRT-PCR reactions (20 µl) were prepared by adding 900 nM of the respective primer pair, 10 µl 2x FastStart Universal SYBR Green Master

(Roche) and 10 ng cDNA template. The following qRT-PCR program was used: a hold step at 95 °C for 15 min followed by 40 cycles of 95 °C for 15 s, 62 °C for 30 s and 72 °C for 30 s. Primer sequences are described in Table S2.

Amplification cycles and PCR efficiencies were determined using LinRegPCR 12 program (BioGazelle). Differential expression ratios were calculated using the Ct difference formula [34].

Determination of hyphal diameter distribution

C. cinerea AmBm *cgl2p*-dTom was grown into a microfluidic device as described above, but incubation at 37 °C was prolonged to 72 h so that the fungus had completely covered the acropetal monitoring area. Bright field images were acquired in the acropetal monitoring area and around 250 hyphal diameters were measured by hand using the straight line tool in Fiji (ImageJ software). Data from two independent experiments were pooled. For the diameter of transporting hyphae, data of several independent experiments (defense-induced hyphae as well as 2-NBDG transporting hyphae) were pooled. Normal distribution of hyphal diameters was tested using the Shapiro-Wilk's test with a 95 % confidence interval in GraphPad Prism (GraphPad Software, USA). None of the experiments passed the normality test. 2-Step clustering analysis was performed using SPSS Statistics Software (IBM). One-way ANOVA with Bonferroni correction was performed to test if one of the three hyphal subpopulations and hyphae, capable of long distance transport, were statistically similar.

Fluorescence bleaching and generation of kymograph

A. avenae was added into the confrontation area of a microfluidic device containing the *C. cinerea* AmBm *cgl2p*-dTom reporter strain for 24 h to induce dTomato expression. A propagating hypha in the acropetal monitoring area was chosen for bleaching. Bleaching was performed on a Zeiss LSM780 confocal microscope with 100 iterations using the maximum laser intensity either once or repeatedly every 20 sec and images were acquired every 2 sec thereafter. The Fiji segmented-line tool was used to trace the induced hypha throughout the imaging frame. To generate a fluorescence profile of the bleached hypha over time (kymograph), the Fiji Reslice tool was used. The kymograph displays the change in fluorescence intensity along the

bleached hypha as a function of time. The grey values of the traced hyphae were exported for the indicated time points and blotted over the length of the hypha to determine responsive compartments.

Analysis of time-lapse image series

Absolute fluorescence intensities were measured at each time point within a time-lapse image series. To acquire a measurement, the Fiji tool "rectangular" was used to create a square region of interest (ROI), which was placed exactly on the hypha of interest (covering the complete diameter of the hypha). To measure the relative fluorescence intensity, the background fluorescence intensity was estimated by placing the same square ROI next to the hypha. The value of the absolute fluorescence intensity within the hypha was then divided by the background fluorescence intensity. This was repeated three times to yield an average value for one hypha. Values in arbitrary units (AU) were subsequently plotted as a function of time.

For 2-NBDG transport, fluorescence intensity measurements were performed additionally for all hyphae within an ROI covering most of the acropetal or basipetal monitoring area. To this end, the fluorescent image was thresholded and a mask created for all hyphae within the ROI. The fluorescence intensity was measured for all hyphae within the mask, summed and plotted against time. In Figure 3, 0.5 AUs were added to simplify visualization within the graphs for the individual control hyphae, as well as for the background and the ROIs. Similarly in Figure 4 and Figure S4, 0.05 AU and 0.5 AU were added for the dTomato fluorescence data sets to aid visualization. Experiments were excluded due to the following: no transport into acropetal or basipetal monitoring area visible, background fluorescence too high, induction of dTomato expression/intra-hyphal NBDG signal too low.

Phase mapping and cross-correlation analysis

The data manipulation was performed using a free Matlab package available at https://markfricker.org/77-2/software/redox-ratio-analysis/redox-ratio-analysis-software-download/ (access July, 2016) [10] and the MapleSoft™ software package CrossCorrelation for cross-correlation analysis. The signal-to-noise ratio of the time series was improved using spatial and temporal averaging with 7x7 and 5x5 pixel

kernel for each pixel and detrended with rolling average of 30, additionally a Hanning window was applied prior to a Discrete Fourier transform with a padding of 128 to extract better phase profiles for dTomato and 2-NBDG.

Fluorescent intensity values of hyphae 1 and 2 and hypha 1 plotted in Fig 4 B and E, respectively, were used for cross-correlation analysis between dTomato and 2-NBDG signals.

Generation of diffusion model

The one dimensional, one directional diffusion was modelled using analytical solution from [2] (equation 2.26). This model allows one to study how the concentration of a substance, characterized by a given diffusion constant D, evolves in time when it diffuses from a source, with a constant concentration $c=1$ (arbitrary units), inside e.g. linear hyphae (one dimensional, open system with concentration c of a substance equal 0 at time $t=0$ (s)). The model (Figure S5) was solved for several positions starting at 300 μm from the source bath for two substances characterized by D_1 and D_2 (which corresponds to a diffusion of a protein and an ion, respectively in a hypha [1]).

To determine the flow kinetics for dTomato and 2-NBDG in propagating hyphae, mean grey values were determined for two different points along the hypha (distance between the points is indicated in the graph). The hyphae were each chosen from two representative time-lapse experiments (Figure 2 and Figure S4A for dTomato and Figure 3 for 2-NBDG).

Statistical analysis

SPSS Statistics Software (IBM) was used for 2-step clustering analysis and Matlab software (MathWorks®, USA) was used for cross-correlation analysis. For all other statistical analyses, GraphPad Software, USA was used. Details regarding all statistical analyses performed and software used can be found in the supplementary table S3, the main text and the respective figure legends.

Supplemental video titles and legends

Video S1. *A. avenae* feeding on *C. cinerea* AmBm *cgl2p*-dTom. Related to Figures 1A and S1C. Video of *A. avenae* feeding on *C. cinerea* AmBm *cgl2p*-dTom. Time-lapse series was acquired with 500 ms between successive frames. The video was compressed to 687 x 559 pixels and was recorded at 3 fps.

Video S2. Oscillation of dTomato fluorescence in acropetal/basipetal trunk hyphae. Related to Figure 2A. Time-lapse video for Figure 2A. *A. avenae* was introduced into the confrontation area of a microfluidic device containing the *C. cinerea* AmBm *cgl2p-dTom* reporter strain 16 h prior to image acquisition. After this preincubation period, a time-lapse image series with a 30 min interval between successive frames was recorded and compressed to 500 x 183 pixels. The video was recorded at 5 fps. Direction of hyphal growth is from left to right. Images corresponding to the confrontation area (middle area) were omitted from the video.

Figure 1

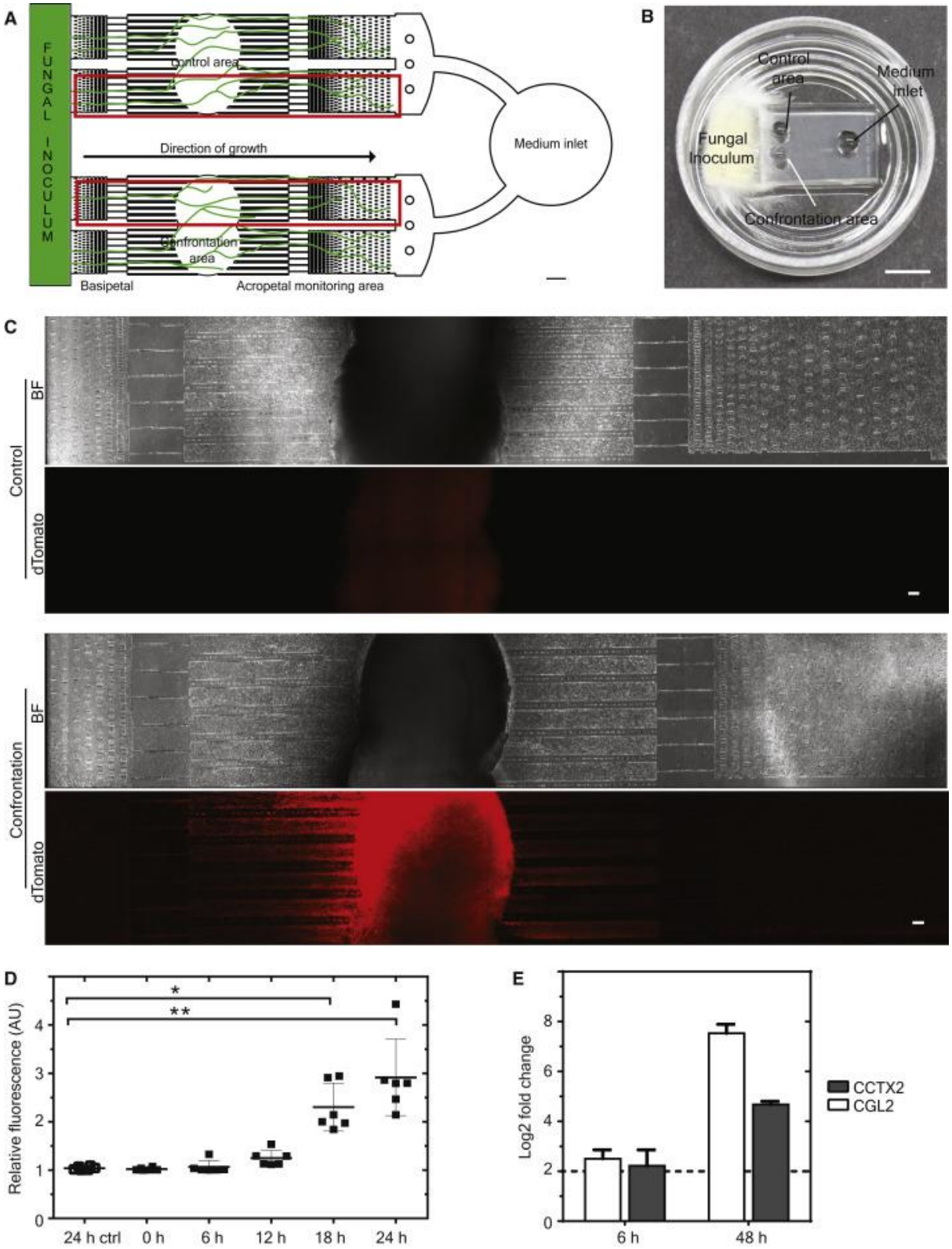
A
FUNGAL INOCCULUM
Control area
Direction of growth
Confrontation area
Medium inlet
Basipetal
Acropetal monitoring area
B
Control area
Medium inlet
Fungal Inoculum
Confrontation area
C
Control
BF
dTomato
Confrontation
BF
dTomato
D
Relative fluorescence (AU)
*
**
24 h ctrl
0 h
6 h
12 h
18 h
24 h
E
Log2 fold change
CCTX2
CGL2
6 h
48 h

Figure 2

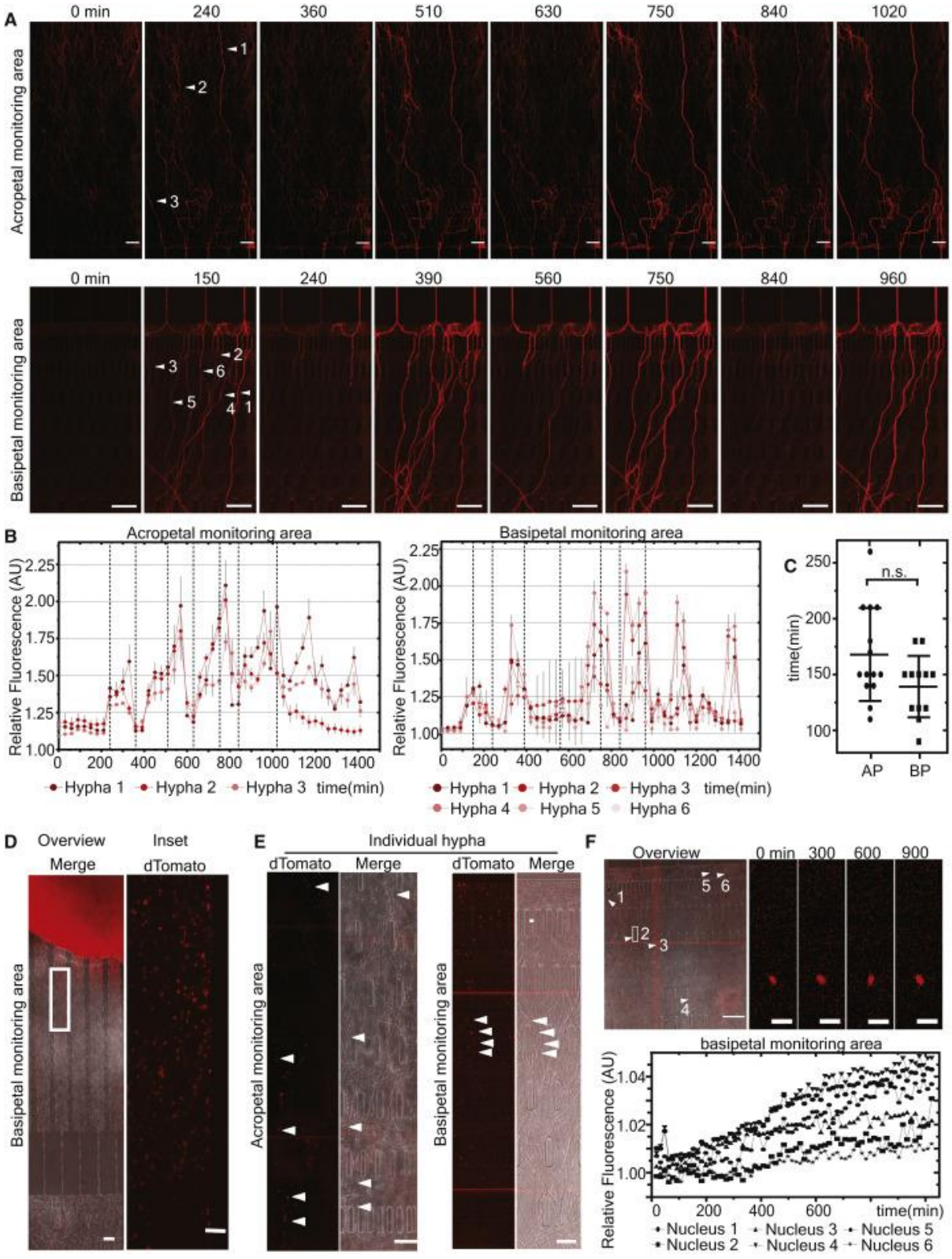
A
0 min
240
360
510
630
750
840
1020
Acropetal monitoring area
1
2
3
0 min
150
240
390
560
750
840
960
Basipetal monitoring area
3
2
6
5
4
1
B
Acropetal monitoring area
Relative Fluorescence (AU)
2.25
2.00
1.75
1.50
1.25
1.00
0
200
400
600
800
1000
1200
1400
Hypha 1
Hypha 2
Hypha 3
time(min)
Basipetal monitoring area
Relative Fluorescence (AU)
Hypha 1
Hypha 2
Hypha 3
time(min)
Hypha 4
Hypha 5
Hypha 6
C
250
200
150
100
time(min)
n.s.
AP
BP
D
Overview
Merge
Inset
dTomato
Basipetal monitoring area
E
Individual hypha
dTomato
Merge
dTomato
Merge
Acropetal monitoring area
Basipetal monitoring area
F
Overview
0 min
300
600
900
5
6
1
2
3
4
basipetal monitoring area
Relative Fluorescence (AU)
1.04
1.02
1.00
0
200
400
600
time(min)
Nucleus 1
Nucleus 2
Nucleus 3
Nucleus 4
Nucleus 5
Nucleus 6

Figure 3

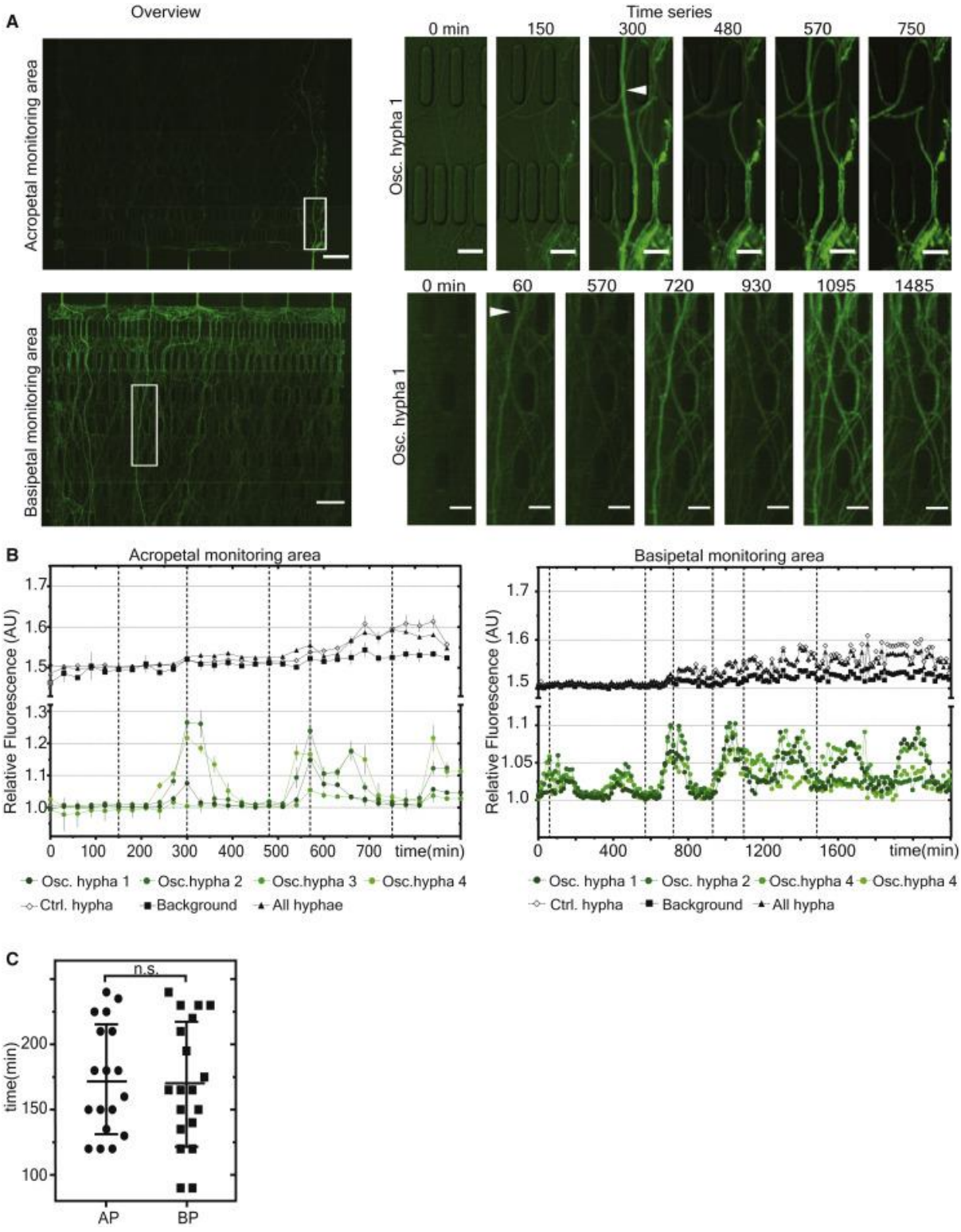
A
Overview
Time series
Acropetal monitoring area
Basipetal monitoring area
Osc. hypha 1
0 min
150
300
480
570
750
60
570
720
930
1095
1485
B
Acropetal monitoring area
Basipetal monitoring area
Relative Fluorescence (AU)
time(min)
Osc. hypha 1
Osc.hypha 2
Osc.hypha 3
Osc.hypha 4
Ctrl. hypha
Background
All hyphae
All hypha
C
n.s.
time(min)
AP
BP

Figure 4

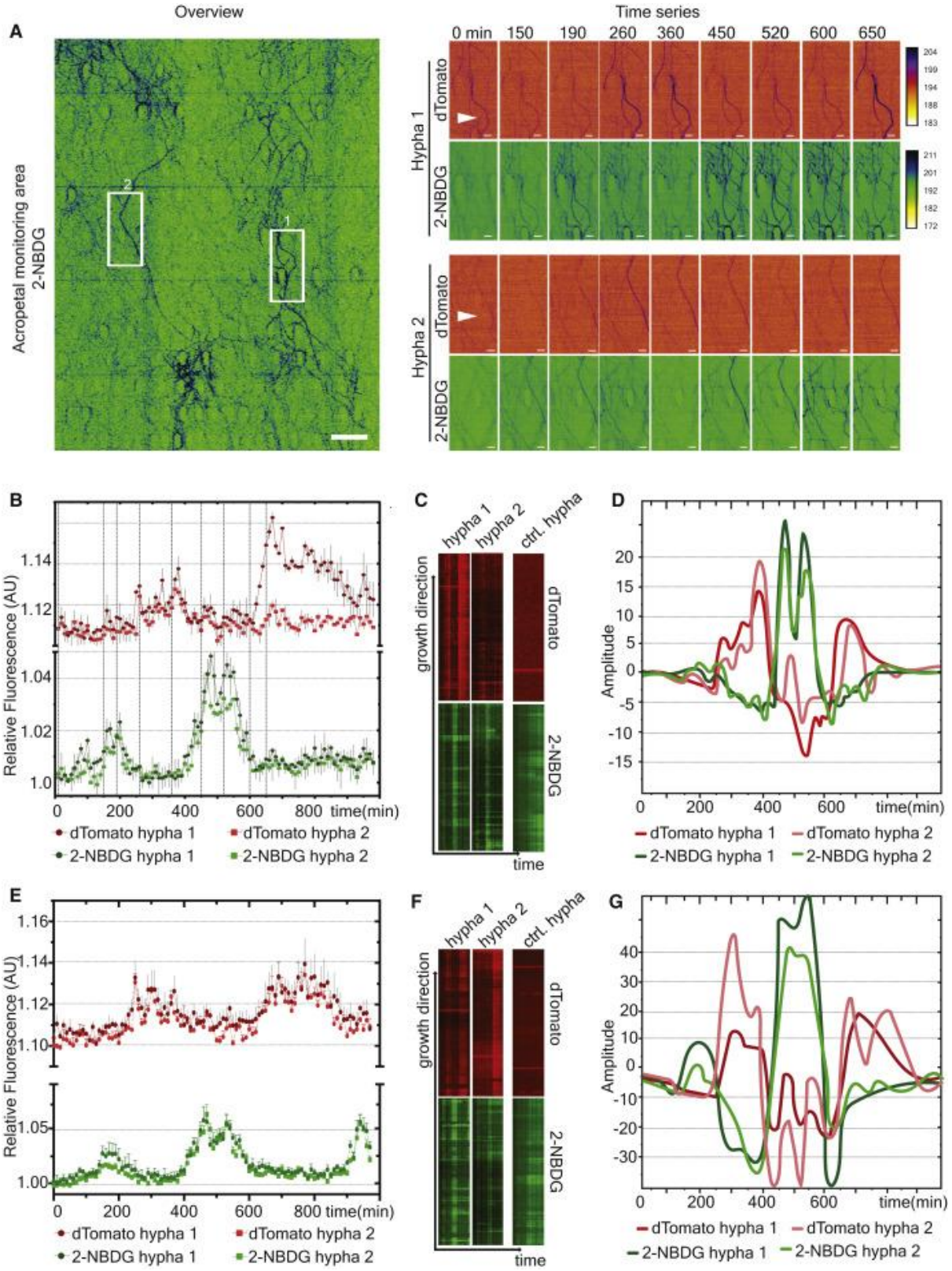
A
Overview
Acropetal monitoring area
2-NBDG
Time series
0 min
150
190
260
360
450
520
600
650
Hypha 1
dTomato
2-NBDG
Hypha 2
dTomato
2-NBDG
B
Relative Fluorescence (AU)
time(min)
dTomato hypha 1
dTomato hypha 2
2-NBDG hypha 1
2-NBDG hypha 2
C
hypha 1
hypha 2
ctrl. hypha
growth direction
dTomato
2-NBDG
time
D
Amplitude
time(min)
dTomato hypha 1
dTomato hypha 2
2-NBDG hypha 1
2-NBDG hypha 2
E
Relative Fluorescence (AU)
time(min)
dTomato hypha 1
dTomato hypha 2
2-NBDG hypha 1
2-NBDG hypha 2
F
hypha 1
hypha 2
ctrl. hypha
growth direction
dTomato
2-NBDG
time
G
Amplitude
time(min)
dTomato hypha 1
dTomato hypha 2
2-NBDG hypha 1
2-NBDG hypha 2

Figure 5

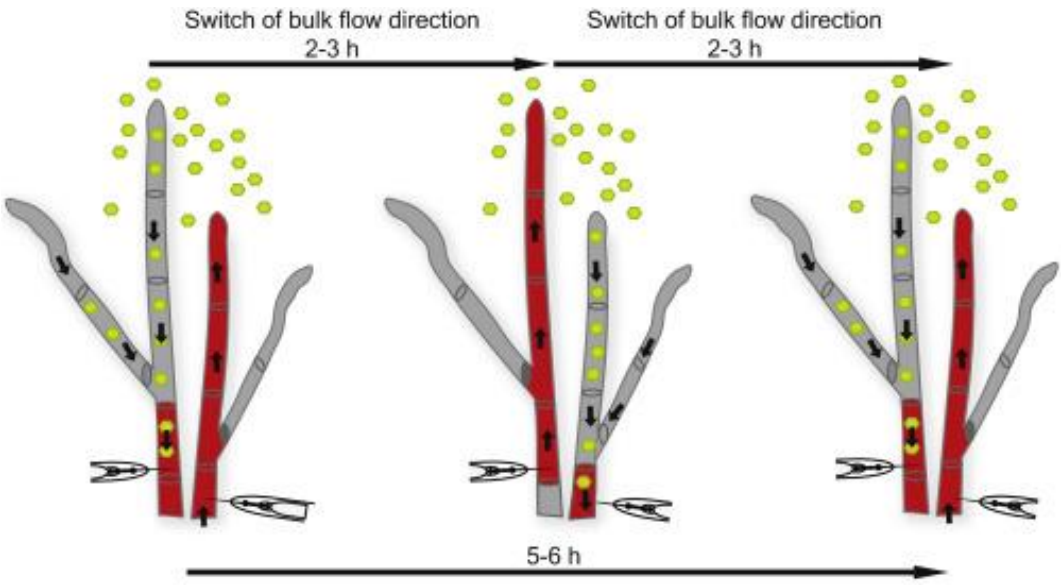
Switch of bulk flow direction
2-3 h
Switch of bulk flow direction
2-3 h
5-6 h

Current Biology, Volume *29*

Supplemental Information

Bidirectional Propagation of Signals and Nutrients in Fungal Networks via Specialized Hyphae

Stefanie S. Schmieder, Claire E. Stanley, Andrzej Rzepiela, Dirk van Swaay, Jerica Sabotič, Simon F. Nørrelykke, Andrew J. deMello, Markus Aebi, and Markus Künzler

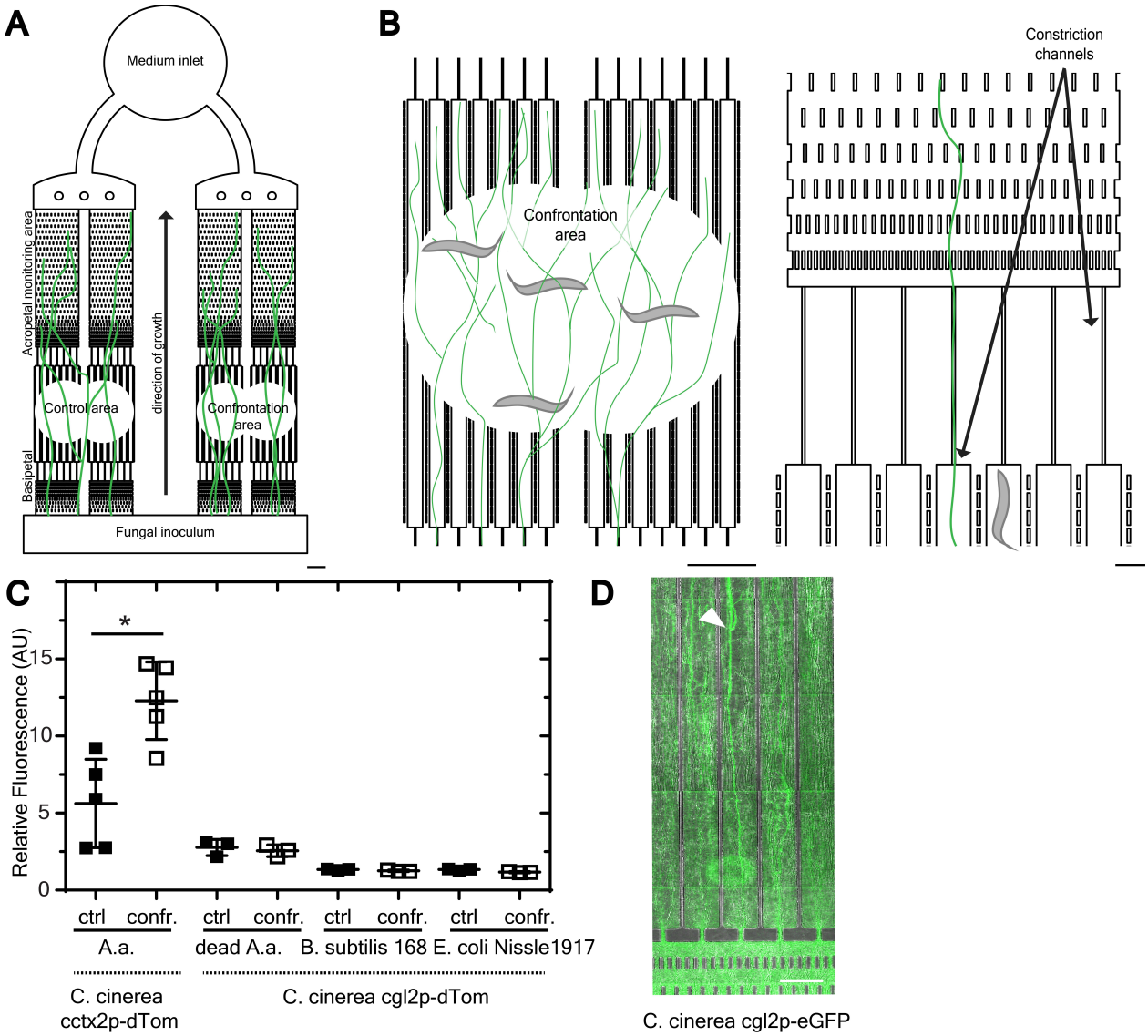

Figure S1. *A. avenae*-specific induction of *cgl2* promoter in *C. cinerea*. Related to Figure 1. (A) Overview of a second FNI device used in this study with a prolonged acropetal monitoring area and shortened confrontation area. Single hyphae (green lines) originating from the agar block with pre-cultivated *C. cinerea* mycelium (fungal inoculum) can be observed and followed over 72 h. Scale bar = 500 µm. (B) Close-up of the confrontation area (left, Video S1) and constriction channels (right). The constriction channels have a height and width of 10 µm and length of 500 µm, thus allowing penetration of individual hyphae but excluding *A. avenae* from entering the basipetal and acropetal monitoring areas. Scale bars = 200 µm. (C) Specificity of the *C. cinerea* defense response. The dTomato fluorescence intensity in the control and confrontation areas was monitored using different inducing agents and respective *C.*

cinerea AmBm dTomato reporter strains and respective fluorescence mean grey values were quantified. *C. cinerea* AmBm *cctx2p-dTom*: 24 h post inoculation with (living) *A. avenae*. Dead *A. avenae*: *C. cinerea* AmBm *cgl2p*-dTom reporter strain 48 h post inoculation with heat-killed *A. avenae*. *E. coli* Nissle and *B. subtilis* 168: *C. cinerea* AmBm *cgl2p*-dTom reporter strain 48 h after 20 µl of respective bacterial culture (OD_{600} = 0.8) were added to the confrontation area. Panel shows three independent experiments, relative fluorescence (mean grey values) of the confrontation and control area are plotted. Mann-Whitney test was performed. The asterisk (*) indicates a p-value of <0.05. Error bars indicate standard deviations. (D) Propagation of defense gene induction is independent of the fluorescent protein used. A microfluidic device containing the *C. cinerea* AmBm *cgl2p-eGFP* reporter strain was inoculated with *A. avenae* and basipetal propagation of the GFP fluorescence signal was monitored. Image was taken 24 h post inoculation with nematodes. The arrowhead indicates propagating hyphae. Scale bar = 100 µm.

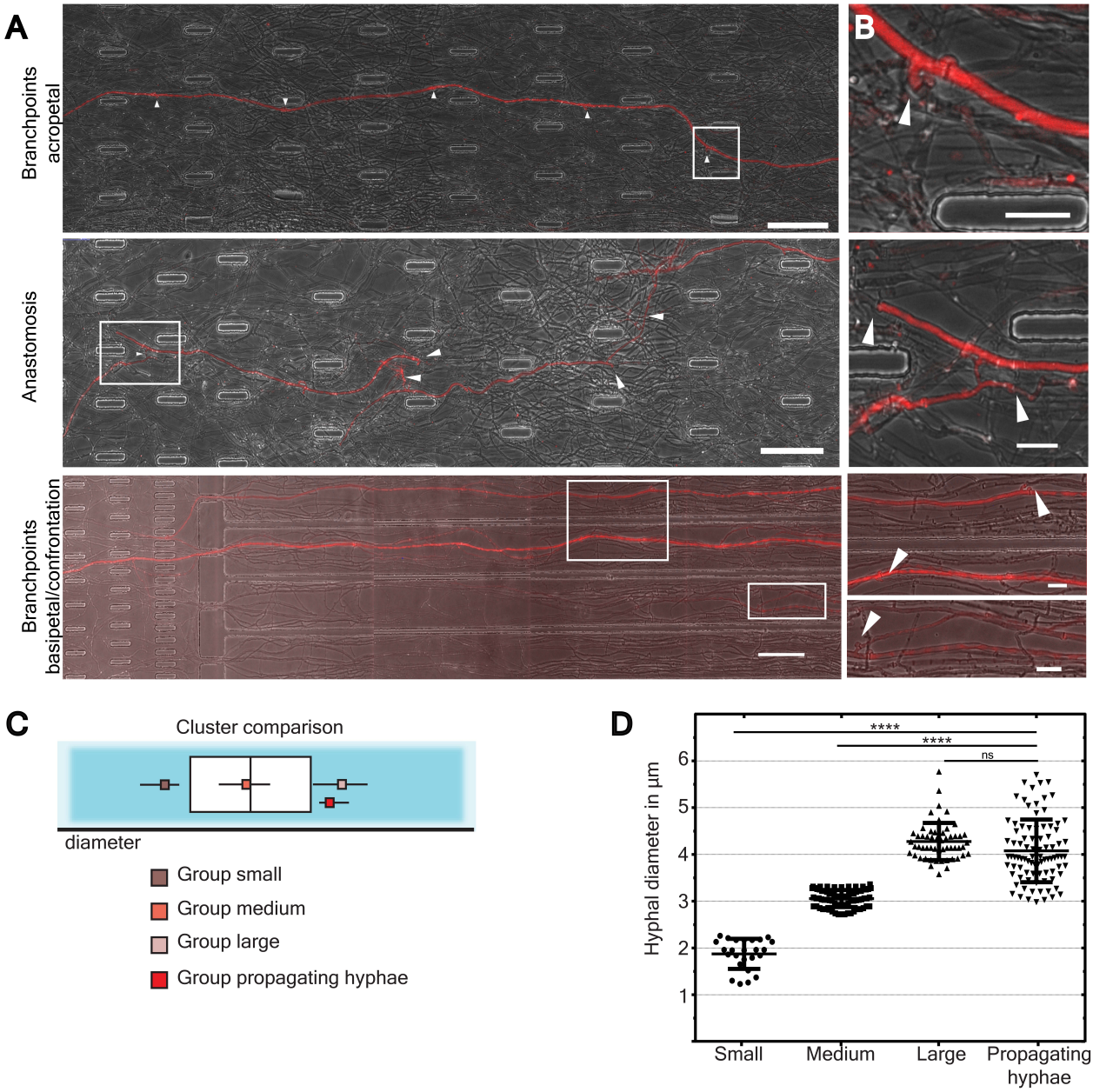

Figure S2. Long distance propagation of *cgl2p*-dTomato induction in distinct hyphae of *C. cinerea*. Related to Figure 2. (A) *A. avenae* was introduced into the confrontation area of a microfluidic device containing the *C. cinerea* AmBm *cgl2p-dTom* reporter strain 16 h before monitoring the dTomato fluorescence intensity. The acropetal monitoring area is shown. Branch points: long distance propagation of the dTomato fluorescence signal in an individual hypha occurs only along the leading trunk hypha and is rarely propagated into a branch. Arrowheads indicate septa and branching points of the trunk hypha. Scale bar = 100 µm. Anastomosis: arrowheads indicate an anastomosis bridge between two leading hyphal trunks. The basipetal monitoring area is shown.

Branch points: propagation of dTomato fluorescence signal from secondary branch into a trunk hypha. Scale bar = 100 µm. (B) Zoom in of branch points and the anastomosis bridge depicted in the white box in (A). Scale bar = 20 µm. (C, D) Distinction of propagating hyphae with regard to their diameter. Diameters of approximately 250 hyphae of *C. cinerea* AmBm *cgl2p-dTom* colonies from two independent experiments, incubated in a microfluidic device for 32 h were determined using the Fiji straight line tool. 2-step clustering analysis revealed three distinct hyphal populations with regard to their diameter in the vegetative mycelium of *C. cinerea* AmBm *cgl2p*-dTom. The populations are displayed in the cluster comparison in (C). The white box represents the 75% quantile of the overall population of measured hyphal diameters with the median. The three populations are indicated with their respective standard deviations. “Group small” has a median of 2.01 µm (27.6%, brown square), “group medium” a median of 3.02 µm (42.5%, orange square) and “group large” a median of 4.21 µm (29.9%, taupe square). The average diameter of hyphae propagating the *cgl2p-dTom* induction is displayed (red square) and has a median of 4 µm. These hyphae thus group into the subpopulation of hyphae having a large diameter. (D) One-way ANOVA with Bonferroni correction was performed to test if the three hyphal subpopulations and hyphae, capable of long distance transport, were statistically different. The (****) asterisk indicates p-value of < 0.0001. Error bars indicate standard deviations.

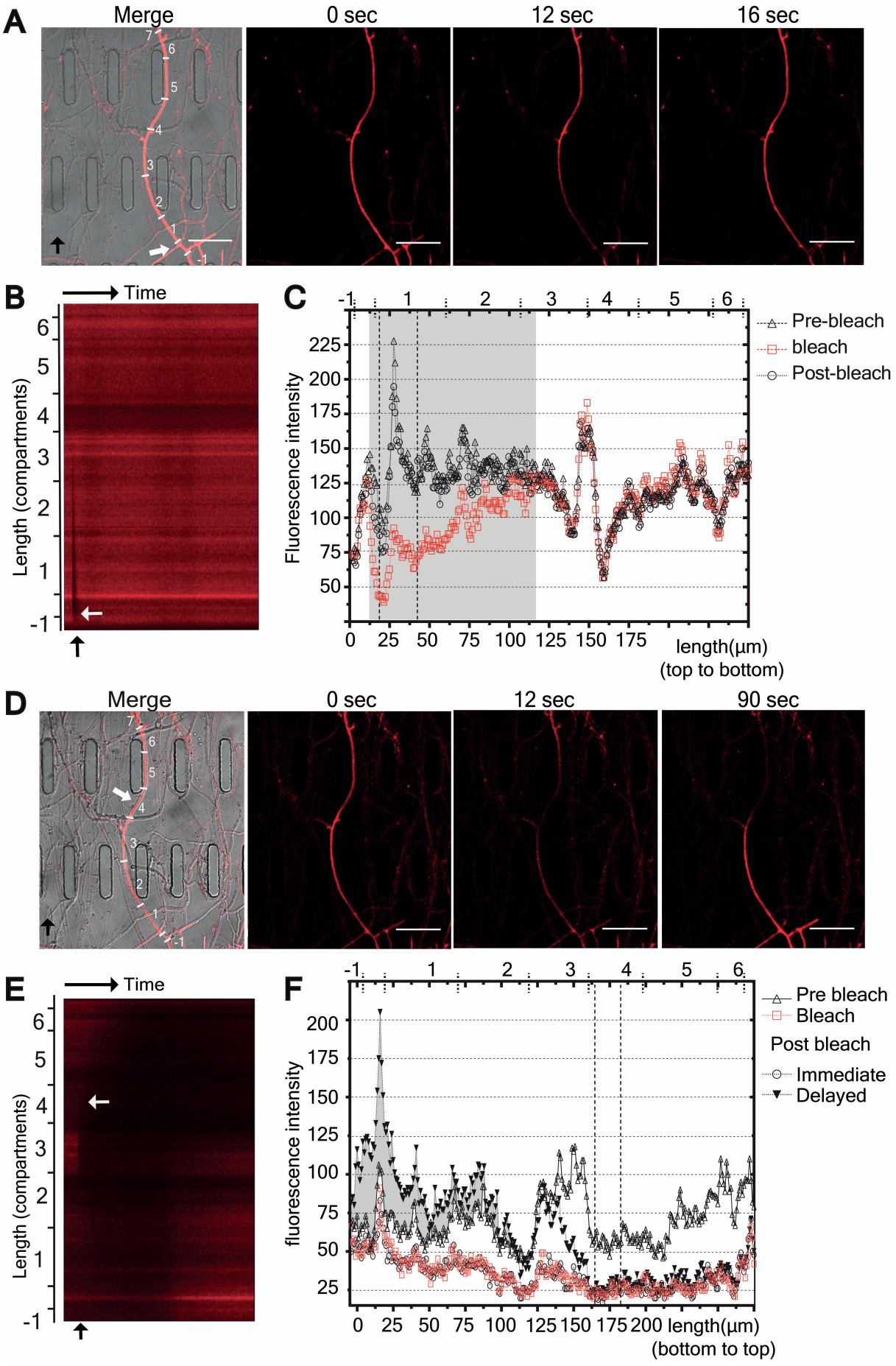
A
Merge
0 sec
12 sec
16 sec
B
Time
Length (compartments)
C
Fluorescence intensity
Pre-bleach
bleach
Post-bleach
length(µm)
(top to bottom)
D
Merge
0 sec
12 sec
90 sec
E
Time
Length (compartments)
F
fluorescence intensity
Pre bleach
Bleach
Post bleach
Immediate
Delayed
length(µm)
(bottom to top)

Figure S3. Fluorescence dynamics of induced hyphae. Related to Figure 2. (A) Fluorescence recovery after bleaching. A hypha induced in the acropetal region was bleached with 100 iterations and images were acquired every 2 sec. Representative images directly before (0 sec) and 12 and 16 sec after the bleaching event are displayed. The merged image shows the location of the septa (white bar) as well as the positions where the fluorescence intensity was measured (the numbers correspond to those in (B) and (C)). The white arrow indicates the bleach point and the black arrow indicates growth direction. Scale bar = 50 µm. (B) Kymograph of the hypha bleached in (A). The kymograph displays the change in fluorescence intensity along the bleached hypha as a function of time. Using the free-line tool in Fiji, a line spanning the bleached hypha was drawn, starting at the -1 compartment, and the fluorescence profile over time along this line was plotted as a kymograph. Individual compartments are labeled according to (A). The bleaching area is indicated by the white arrow, while the bleaching time point is indicated by the black arrow. (C) Quantification of fluorescence intensity along the hypha bleached in (A) as a function of the growth direction starting at the -1 compartment (= 0 µm) towards the 6th compartment (apical end = 250 µm). Quantification was performed right before (0 sec, 'pre-bleach') and 12 ('bleach') and 16 sec ('post-bleach') after the bleaching event. The bleaching area is indicated by the dashed lines. The grey area indicates the compartments that responded to the bleaching event. (D) The same hypha was bleached again after a recovery phase of 30 min. This time bleaching was performed repeatedly every 20 sec, to completely deplete dTomato in respective area (see (E)). Time course as in (A), white arrow indicates the bleaching area and black arrow the growth direction. Scale bar = 50 µm. Note that during the time course the septal opening state is changing for septa connecting compartments 3 and 4. The septa connecting compartment 1 and -1 has opened since the time-lapse experiment in (A). (E) Kymograph as in (B) shows the opening of septa and streaming of dTomato into the imaging region originating from the confrontation area. The septum connecting compartments -1 and 1 is open compared to bleaching experiment in (A) and the septum connecting compartments 3 and 4 is closing during the time course, preventing transport of dTomato. (F) Quantification of the fluorescence intensity along the bleached hypha as in (C), for time points directly before (0 sec, 'pre-bleach'), after (16 sec, 'immediate') and 90 sec ('delayed') after the bleaching event. The grey area corresponds to compartments

displaying higher fluorescence intensities than before the bleaching event. The dashed line indicates the position of the bleaching area.

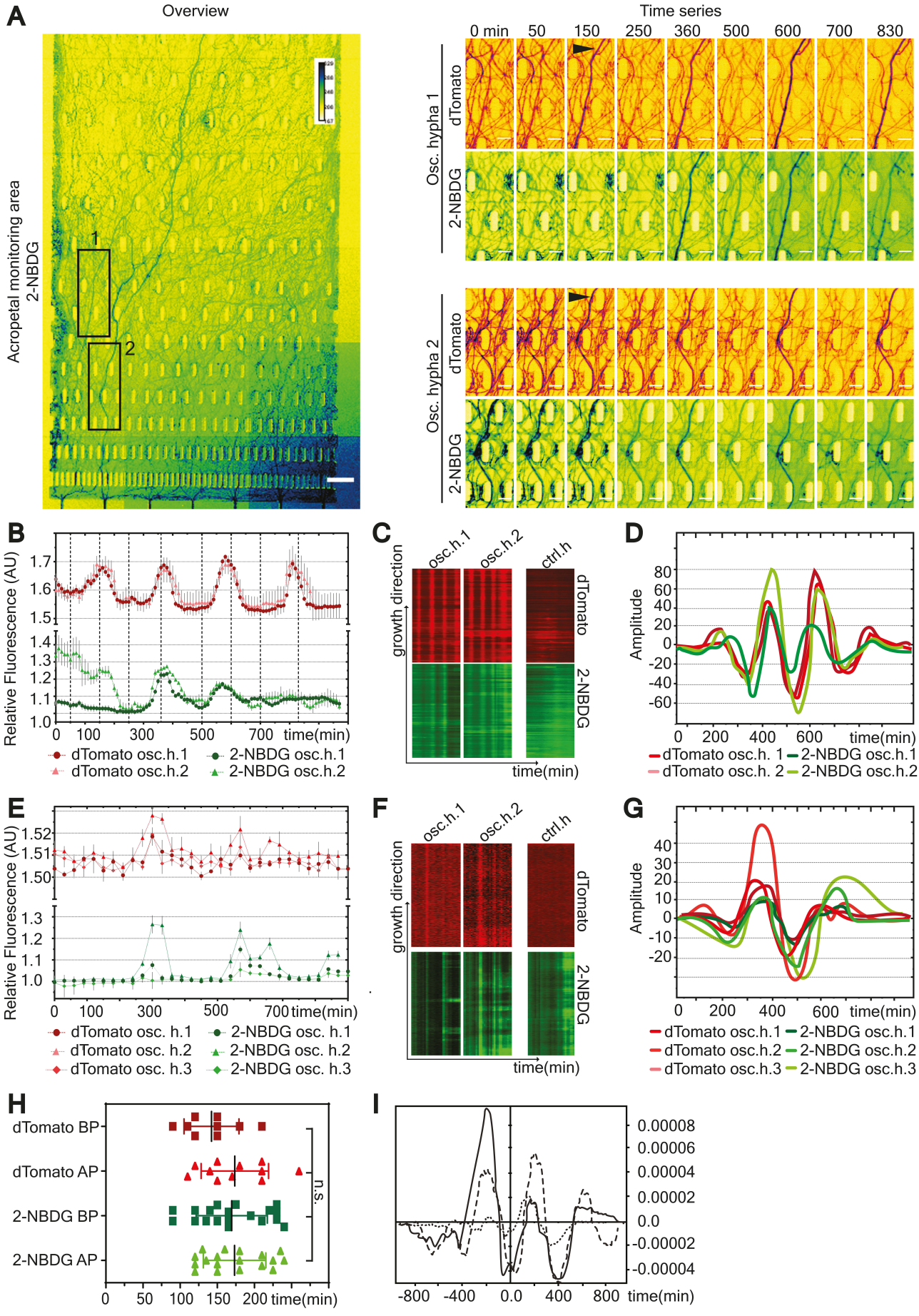
A
Overview
Acropetal monitoring area
2-NBDG
1
2
Time series
0 min
50
150
250
360
500
600
700
830
Osc. hypha 1
dTomato
2-NBDG
Osc. hypha 2
dTomato
2-NBDG
B
Relative Fluorescence (AU)
time(min)
dTomato osc.h.1
dTomato osc.h.2
2-NBDG osc.h.1
2-NBDG osc.h.2
C
osc.h.1
osc.h.2
ctrl.h
growth direction
dTomato
2-NBDG
time(min)
D
Amplitude
time(min)
dTomato osc.h. 1
dTomato osc.h. 2
2-NBDG osc.h.1
2-NBDG osc.h.2
E
Relative Fluorescence (AU)
time(min)
dTomato osc. h.1
dTomato osc. h.2
dTomato osc. h.3
2-NBDG osc. h.1
2-NBDG osc. h.2
2-NBDG osc. h.3
F
osc.h.1
osc.h.2
ctrl.h
growth direction
dTomato
2-NBDG
time(min)
G
Amplitude
time(min)
dTomato osc.h.1
dTomato osc.h.2
dTomato osc.h.3
2-NBDG osc.h.1
2-NBDG osc.h.2
2-NBDG osc.h.3
H
dTomato BP
dTomato AP
2-NBDG BP
2-NBDG AP
n.s.
time(min)
I
time(min)

Figure S4. Concomitant propagation of 2-NBDG and dTomato fluorescence. Related to Figures 3, 4 and 5. *A. avenae* was added into the confrontation area of a microfluidic device containing the *C. cinerea* AmBm *cgl2p-dTom* reporter strain 24 h prior to the addition of 30 µM 2-NBDG to the same area. A time-lapse image series in the acropetal monitoring area was acquired to determine whether long-distance propagation of dTomato and 2-NBDG fluorescence signals occurs in the same hyphae. (A) Overview of the 2-NBDG fluorescence intensity in the acropetal monitoring area around 6 h post addition of 2-NBDG to the confrontation area. Two regions of interest comprising exemplary propagating hyphae were selected and changes in dTomato and 2-NBDG fluorescence intensities were monitored for both hyphae over time. The images were false colored using the inverted Green FIRE blue LUT (2-NBDG) and the inverted FIRE LUT (dTomato). Arrowheads indicate the hyphae monitored and the positions at which the quantification in (B) was performed. Scale bars = 100 µm (overview) and 25 µm (time series). (B) Graph showing the relative dTomato and 2-NBDG fluorescence intensities of the selected hyphae in the acropetal monitoring area over time. Error bars represent SDs. (C) Kymograph for the two hyphae of interest in (A) and (B) and a control (non-oscillating) hypha, note the increase in 2-NBDG fluorescence over time for the control hypha, absent for the oscillating hyphae. Hyphae were traced in growth direction over the whole field of view and fluorescence intensity is plotted over time. (D) Overlay of the oscillation behavior shown in (B) after spatial averaging and detrending. The signal-to-noise ratio of the time series was improved using spatial and temporal averaging with a 7x7 and 5x5 pixel kernel and the data was detrended with rolling average of 10 prior to smoothing with a Hanning window. (E) Graph as in (B) for two additional hyphae from a biological replicate, showing the relative dTomato and 2-NBDG fluorescence intensities in the acropetal monitoring area over time. Error bars represent SDs. (F) Kymograph for the two hyphae of interest in (E) and a control (non-oscillating) hypha, note again the increase in 2-NBDG fluorescence over time for the control hypha, absent in the oscillating hyphae. (G) Overlay of the oscillation behavior shown in (E) after spatial averaging and detrending, performed as in (D). (H) Comparison of the duration of an individual period of dTomato and 2-NBDG propagation in each direction. The time of an individual propagation for dTomato and 2-NBDG acropetal (AP) and basipetal (BP) direction displayed in Figure 2C and Figure 3C were combined and tested for statistical difference using one-way ANOVA. (I) Cross-

correlation analysis between the dTomato and 2-NBDG channel was performed for the two hyphae of interest in Figure 4B and hypha 1 in Figure 4E. Full black and dotted (···) lines correspond to hypha 1 and hypha 2 in Figure 4B respectively, the dashed line (- -) to hypha 1 in Figure 4E.

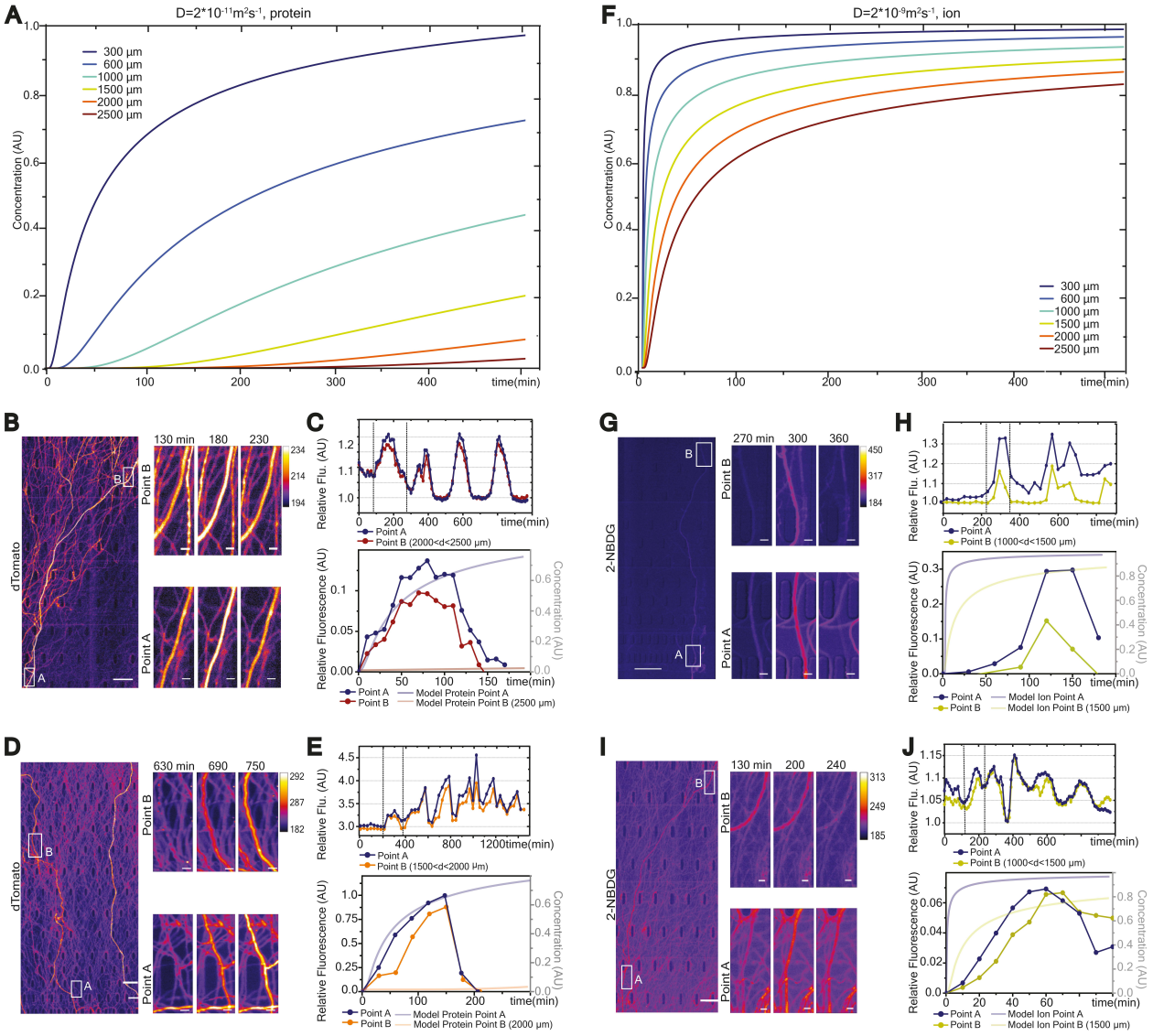

Figure S5. Diffusion model for solutes within hyphae. Related to Figures 4 and 5. Diffusion model of a substance from a source bath within a fungal hypha. The model is adapted to the FNI set-up, with point 0 µm in the model being 300 µm away from the source bath, reflecting observations for the acropetal and basipetal monitoring areas. For different positions within a hypha, with various distances to point 0 µm (colored lines), concentration of a substance is modelled in time (see Star Methods, Generation of diffusion model for details). (A) The panel shows the diffusion model of a typical protein (25kDa) (diffusion coefficients taken from [S1]). (B) Fluorescence profile of dTomato over time for two points A and B along a propagating hypha for a representative experiment. The panel shows overview and time series for the two points A and B indicated in the overview. (C) Upper graph shows the respective fluorescence

profile for points A and B (defined in (B)) over time. The first cycle of fluorescence increase (dashed lines) is normalized to zero and plotted together with the theoretical values for the 25 kDa model protein diffusion in the lower graph. The distance between points A and B is indicated and color-coded in both graphs. The theoretical fluorescence values for the model protein correspond to the distance between A and B and are correspondingly color-coded in a lighter hue. The scale bar of 'Concentration (AU)' can have a maximum value of 1. (D) The fluorescence profile of dTomato over time for a second representative experiment is displayed, with the panel showing an overview and a time series for two points A and B along the induced hypha (as in (B)). (E) Analysis of data displayed in (D) as detailed in (C). (F) The panel shows diffusion behavior of a typical ion (diffusion coefficients taken from [S1]) as an approximation for 2-NBDG (342 Da). (G) Fluorescence profile of 2-NBDG over time for two points A and B along a propagating hypha for a representative experiment. Panel shows overview and time series for the two points indicated in the overview. (H) Upper graph shows the respective fluorescence profile for A and B (defined in (G)) over time. The first cycle of fluorescence increase (dashed lines) is normalized to zero and plotted together with the theoretical values for model ion diffusion in the lower graph. The distance between points A and B is indicated and color-coded in both graphs. The theoretical fluorescence values for the model ion correspond to the distance between A and B and are correspondingly color-coded in a lighter hue. The scale bar of 'Concentration (AU)' can have a maximum value of 1. (I) Fluorescence profile of 2-NBDG over time for two points A and B along a propagating hypha in a second representative experiment as compared to (G). (J) Analysis of data displayed in (I) as detailed in (H). Images were false colored using the FIRE lookup table. Scale bars = 100 μm (overview) and 10 μm (time series).

Strain	**Genotype**	**Phenotype**	**Source**
Coprinopsis cinerea AmBm	*A43mut B43mut pab1.2*	PABA-auxotroph, homodikaryon	[S2]
Coprinopsis cinerea AmBm *cgl2p*-dTom	Integrated plasmid pMA541	Expression of cytoplasmic dTomato under control of *cgl2p*	This study
Coprinopsis cinerea AmBm *cctx2p*-dTom	Integrated plasmid pMA1101	Expression of cytoplasmic dTomato under control of *cctx2p*	This study
Coprinopsis cinerea AmBm *cgl2p*dTomH1	Integrated plasmid pMA1130	Expression of nuclear localized version of dTomato under control of *cgl2p*	This study
Coprinopsis cinerea AmBm *cgl2p*-eGFP	Integrated plasmid pMA1131	Expression of cytoplasmic eGFP under control of *cgl2p*	This study
Aphenlenchus avenae Bastian	WT		[S3]
Escherichia coli Nissle 1917	WT		[S4]
Bacillus subtilis 168	*trpC2+*		[S5]

Plasmid	**Description**	**Source**
pRS426	2µ-URA3	[S6]
pMA412	pRS426-pAbgpdII-i-*dTomato*-tPcMNP	[S7]
pMA541	pRS426-*cgl2p*-i-*dTomato*-tPcMNP	This study

pMA1131	eGFP construct	This study
pMA1130	pRS426-*cgl2p-dTomato*-H1-tPcMNP	This study
pMA1101	pRS426-*cctx2p-dTomato*-tPcMNP	This study

Table S1. Strains and plasmids used in this study. Related to STAR methods sections 'Strains and general cultivation conditions' as well as 'Generation of *C. cinerea* reporter strains'.

Primer name	**Sequence (5` - 3`)**	**Purpose**	**Source**
Cgl2p for	GTCGGAGGAAAGATGCCAGA AGAAGGGCCCGACACCTTTC CAGGACTGCG	Amplification of *cgl2p* and recombination into pMA412	This study
Cgl2p rev	GTGGTGTACTGACCGCCATG GCGATAAGCTTGGCTTTGAG CTGTAGAACTG		This study
eGFP for	CTCAGTTCTACAGCTCAAAGC CAAGGTAGGCATTCGACTTT CCTCTCATTATC	Amplification of eGFP for recombination into pMA541	This study
eGFP rev	CGGCCGCTCTAGAACTAGTG GATCCGTTTGTGGAAGAACA GTATACATGTATTG		This study
CCTX2p for	CAGAAGAAGGGCCCCCCCTC GAGGTCGAGAGTTGAAAGAA TTGCGGCACGTC	Amplification of *cctx2p*for recombination into pMA541	This study
Cctx2p rev	GGTCGGGCTGTGTGGTGTAC TGACCGCCATGGAAATGACC TACGATGAGTTGAAG		This study
H1 for	CCTGTTCCTGTACGGCATGG ACGAGCTGTACAAGATGTCT ACTGTAGCTGAACC	Amplification of *C. cinerea* AmBm histone 1 and recombination into pMA541	This study
H1 rev	GGTAAGAAACCGCGTGGAAT ATGAATTCAAGCCGTGGTCG CCTATTTCCGG		This study

TubM1Fw	GTCATGTCCGGTATCACCAC	qRT-PCR primer for tubulin (JGI ID: 393528)	[S4]
TubM1Rv	GGGAAAGGAACCATGTGGA	qRT-PCR primer for tubulin (JGI ID: 393528)	[S4]
CGL2_2Fw qRTPCR	ACAATGCGGAGAACTCTTTG T	qRT-PCR primer for CGL2 (JGI ID: 488611)	[S4]
CGL2Rv qRTPCR	CCAGCGAGAATCCTAAGCA	qRT-PCR primer for CGL2 (JGI ID:488611)	[S4]
qPCR_77_f	GGTAGTAGTCGCCTGAATCG	qRT-PCR primer for CCTX2 (JGI ID:369589)	[S4]
qPCR_77_r	CTCCGGTGCAGAGGAATAC	qRT-PCR primer for CCTX2 (JGI ID:369589)	[S4]

Table S2. Primer sequences. Related to STAR methods sections 'Generation of *C. cinerea* reporter strains' and 'Validation of defense gene expression'.

Experiment	# of biological replicates	Statistical analysis
Figure 1 D	N = 6	Kruskal-Wallis one-way ANOVA
Figure 1 E	N = 3	
Figure 2 C	N = 11 (acropetal) N = 8 (basipetal)	Mann-Whitney
Figure 3 C	N = 14 (acropetal) N = 13 (basipetal)	Mann-Whitney
Figure S1 C	N = 3	Mann-Whitney
Figure S2 C and D	N = ~ 250 (hyphae) 2 independent experiments combined 2-NBDG/dTomato propagating hyphae are pooled from > 20 independent experiments	2-step cluster analysis One-way ANOVA with Bonferroni correction
Figure S4 H	Combined data Figure 2 C and Figure 3 C	Kruskal-Wallis one-way ANOVA

Table S3. Number of biological replicates and statistical analysis. Relates to Figure 1, 2 and 3, Figures S1, S2 and S4, as well as STAR method section 'Statistical analysis'.

Supplemental References

S1. Fricker, M.D., Heaton, L.L.M., Jones, N.S., and Boddy, L. (2017). The Mycelium as a Network. Microbiol Spectr *5*.

S2. Swamy, S., Uno, I., and Ishikawa, T. (1984). Morphogenetic Effects of Mutations at the a and B Incompatibility Factors in Coprinus-Cinereus. Journal of General Microbiology *130*, 3219-3224.

S3. Bleuler-Martinez, S., Butschi, A., Garbani, M., Walti, M.A., Wohlschlager, T., Potthoff, E., Sabotic, J., Pohleven, J., Luthy, P., Hengartner, M.O., et al. (2011). A lectin-mediated resistance of higher fungi against predators and parasites. Mol Ecol *20*, 3056-3070.

S4. Plaza, D.F., Schmieder, S.S., Lipzen, A., Lindquist, E., and Kunzler, M. (2015). Identification of a Novel Nematotoxic Protein by Challenging the Model Mushroom Coprinopsis cinerea with a Fungivorous Nematode. G3 (Bethesda) *6*, 87-98.

S5. Kunst, F., Ogasawara, N., Moszer, I., Albertini, A.M., Alloni, G., Azevedo, V., Bertero, M.G., Bessieres, P., Bolotin, A., Borchert, S., et al. (1997). The complete genome sequence of the gram-positive bacterium Bacillus subtilis. Nature *390*, 249-256.

S6. Christianson, T.W., Sikorski, R.S., Dante, M., Shero, J.H., and Hieter, P. (1992). Multifunctional yeast high-copy-number shuttle vectors. Gene *110*, 119-122.

S7. Stanley, C.E., Stockli, M., van Swaay, D., Sabotic, J., Kallio, P.T., Kunzler, M., deMello, A.J., and Aebi, M. (2014). Probing bacterial-fungal interactions at the single cell level. Integr Biol (Camb) *6*, 935-945.